



This is a repository copy of *Pollutant and corrosion control technology and efficient coal combustion*.

White Rose Research Online URL for this paper:

<https://eprints.whiterose.ac.uk/115731/>

Version: Accepted Version

Article:

Daood, S.S., Ottolini, M., Taylor, S. et al. (5 more authors) (2017) Pollutant and corrosion control technology and efficient coal combustion. *Energy and Fuels*, 31 (5). pp. 5581-5596. ISSN 0887-0624

<https://doi.org/10.1021/acs.energyfuels.7b00017>

This document is the Accepted Manuscript version of a Published Work that appeared in final form in *Energy and Fuels*, copyright © American Chemical Society after peer review and technical editing by the publisher. To access the final edited and published work see <https://doi.org/10.1021/acs.energyfuels.7b00017>

Reuse

Items deposited in White Rose Research Online are protected by copyright, with all rights reserved unless indicated otherwise. They may be downloaded and/or printed for private study, or other acts as permitted by national copyright laws. The publisher or other rights holders may allow further reproduction and re-use of the full text version. This is indicated by the licence information on the White Rose Research Online record for the item.

Takedown

If you consider content in White Rose Research Online to be in breach of UK law, please notify us by emailing eprints@whiterose.ac.uk including the URL of the record and the reason for the withdrawal request.



eprints@whiterose.ac.uk
<https://eprints.whiterose.ac.uk/>

Pollutant and corrosion control efficient coal combustion technology

Syed Sheraz Daood ^{a,*}, Marc Ottolini ^b, Scott Taylor ^c, Ola Ogunyinka ^a, Md. Moinul Hossain ^d, Gang Lu ^d, Yong Yan ^d, William Nimmo ^a

^{a,*} Energy Engineering Group, Energy 2050, Department of Mechanical Engineering, University of Sheffield, Sheffield, S10 2TN, UK.

^b International Innovative Technologies Ltd, Unit 5, Queens Court, Third Avenue, Team Valley Trading Estate, Gateshead, NE11 0BU, UK.

^c Sembcorp Utilities UK Ltd., Sembcorp UK headquarters, Wilton International, Middlesbrough, TS90 8WS, UK.

^d School of Engineering and Digital Arts, University of Kent, Canterbury, Kent CT2 7NT, UK.

KEYWORDS fuel additive, combustion efficiency, corrosion, flame temperature, NO_x, particulate, slagging, fouling.

ABSTRACT

High efficiency and low emissions from pf coal power stations has been the drive behind the development of present and future efficient coal combustion technologies. Upgrading coal, capturing CO₂, reducing emission of NO_x, SO₂ and particulate matter, mitigating slagging, fouling and corrosion are the key initiatives behind these efficient coal technologies. This study focuses on a newly developed fuel additive (Silanite™) based efficient coal combustion technology, which addresses most of the aforementioned key points. Silanite™ a finely milled

multi-oxide additive when mixed with the coal without the need to change the boiler installation has proven to increase the boiler efficiency, flame temperature with reduction in corrosion, NO_x and particulate matter (dust) emissions. The process has been developed through bench, pilot (100kW_{th}) and full scale (233 MW_{th}). The process has been found to have a number of beneficial effects that add up to a viable retrofit to existing power plant as demonstrated on the 233MW_{th} boiler tests (under BS EN 12952-15:2003 standard). Multifaceted benefits proven on commercial and lab scale included reductions of 20% in the overall particulates, 42% in loss on ignition, 8-25% in NO_x with about 30% increase in the life span of tube section of the boiler.

Corresponding author

* Dr. Syed Sheraz Daood, Room 1.11, Level 1, Arts Tower, Energy Engineering Group, Energy 2050, Department of Mechanical Engineering, University of Sheffield, Sheffield, S10 2TN, UK.

Email: s.daood@sheffield.ac.uk

1. INTRODUCTION

The existing coal-fired power utility operators in the world are implementing ever stricter control regulations. For example, in Europe the European Commission's industrial emissions directive (IED); the USA's the clean power plan (TCPP) and environmental protection bureau china (EPBC). Successful agreements in Paris through the recent COP21 Climate Change summit are leading the way to governments directing their economies toward lower carbon energy usage and power generation. However, in the interim period to decarbonisation, there is a need to continue to operate fossil fuel-fired power stations until a realistic balance of renewable

technologies and nuclear power is achieved¹. World-wide, coal-fired power generation has a 41% share of the total [2]; hence, there is a large opportunity for new technologies to impact on reducing emissions and increasing efficiency. Improvement of combustion efficiency with pollutants reduction (NO_x, SO₂, particulate dust) has been proven with various coal conversion technologies including catalyst / additive based technologies³⁻⁴. The catalyst / additives broadly classified as organic and inorganic are presently used in the power sector as catalysts⁵⁻⁷; however, in general, inorganic additives are widely applied due to the cost to benefit ratios. Recently, many studies have been focused on the utilization of fuel additives to improve combustion and reduce pollutants on the bench to small pilot scales^{4, 7-13}.

The use of these fuel additives economically sourced or formulated could be beneficial to address the following problematic issues associated with coal combustion; 1-emission reduction (NO_x, SO₂, CO₂, CO and dust), 2-fly ash improvement (reducing unburnt carbon and the concentration of challenging ash species, increasing the melting points- ash fusion temperatures and particle size distribution), 3-combustion efficiency improvement (fuel savings, heat release and temperature gain), 4- dust emission reduction- post electrostatic precipitator, 5- resistance towards fireside corrosion.

There have been few recent technical reports published to demonstrate effectiveness of injected additives in the coal stream towards the improvement in inhibition of lignite ash slagging and fouling, coal saving- bed temperature rise- carbon content reduction in fly ash and steam to fuel ratio on 30 MW_{th} industrial pulverized coal-fired boiler¹⁴, 5 MWe circulating fluidized bed boiler¹⁵ and 5 t.h⁻¹ smoke tube boiler¹⁶ respectively. Some other technologies which are based on the injection of the additives in the flue gas pathway i.e. dry sodium bicarbonate¹⁷ based Airborne Process™, Sulphur trioxide-air mixture¹⁸ based Pentol flue gas

conditioning system and dry sorbent (hydrated lime) based injection¹⁹ demonstrate reduction in SO_x-NO_x emissions, resistivity of the electrostatic precipitators (ESP) and emitted acidic gas concentrations, respectively. Moreover economic driven overconsumption of high quality coal sources has resulted in investigation of technologies concentrating on processing coal waste as a main fuel component in thermal power plants. Investigations on the coal water slurry (CWS) and CWS containing petrochemicals (CWSP) based droplet firing technology shows greater potential to work in boilers as main fuel²⁰. This is possible with optimal CWSP blends yielding shortest ignition delays and highest temperature of combustion along with other pollution remedial impact on the environment²⁰. All of the above technologies have been demonstrated to provide part solution up to a restricted scale without multifaceted solution. This knowledge gap is explored in developing an additive based process technology to contribute to scarcely available data linked with findings from research based bespoke test rigs and a large scale commercial boiler (260-280 t.h⁻¹).

For many power plant operators the improved thermal combustion efficiency and the implications for reductions in fuel consumption and emissions are highly significant factors, but for others, the ability to improve the quality of fly ash for re-sale into construction sector applications and resistance towards corrosion will be priorities. Whatever the motivation for power station owners in different parts of the world, the range of proven benefits associated with the Silanite™ fuel technology means that it is extremely well placed in providing multipurpose solution to the individual power station challenges. The research findings of this paper focus especially on the pollutant (NO_x, particulate emissions) and corrosion control with a wider effect on the boiler performance (ash fusibility, slagging/fouling, flame temperature, carbon burnout).

2. MATERIAL AND METHODS

This study focuses on understanding the effectiveness of a newly developed solid pulverised fuel additive (Silanite™) towards NO_x reduction, particulate control, and secondary effects on ash fusibility, slagging and fouling and boiler tube corrosion. Studies are presented from a pilot scale (100 kW_{th}) combustor to commercial scale (233 MW_{th} ~ 260-280 t.h⁻¹ steam output) pulverized fuel boiler. Corrosion studies (1000 h operation) were performed in lab scale furnace test reactors.

2.1. Pilot scale test facility

The combustion test facility (Figure 1a) utilized for the pilot scale tests comprised of 8 x 400 mm (ID) sections with a total of 4 m furnace height and has a down-firing configuration. The throat diameter of the burner is about 66 mm with an overall maximum designed fuel thermal input rating of about 100 kW_{th}. In-flame measurement of CO₂, O₂, NO_x, SO₂ and CO and the exit flue measurements along with temperatures throughout the furnace are recorded through USB high-resolution data acquisition personal daqview modules (Iotech). Further details of the combustion test facility (CTF) have been presented in other studies^{11-12, 21}. The loss in weight twin-screw feeder (Rospen) utilized for coal feeding can feed coal up to 15-20 kg.h⁻¹, and a small vibratory feeder was used to inject fuel additive. The feeder for the additive was calibrated to feed up to approximately 6% by volume or 13% by weight fraction of the coal feed. The fly ash was separated from the flue gas by cyclone separator before emission. The collection efficiency of the cyclone separator is about 96% for particles above 10 microns.

The gas measurements were recorded using chemiluminescence (NO_x), non-dispersive infrared (CO, CO₂) and paramagnetic (O₂) working principle based standard instruments. The collected fly ash samples were subjected to XRF, LOI, Ash fusibility analyses.

2.2. Utility boiler

The utility boiler having the maximum operating steam flow on coal of 260-280 t.h⁻¹, whereas, the minimum steam flow is 170 t.h⁻¹ was selected for the commercial scale testing program. The combustion chamber volume for the boiler is about 1185 m³ having furnace dimensions of 29 m x 7.5 m x 7.6 m with 770 m² to be an effective furnace heating surface exposed to the radiant heat. The throat diameter for all burners is about 650 mm with a total of 12 burners placed in 3 landings at 2440 mm apart between centers. The pf coal is radially fed into the burners with a dedicated separate central coolant core air system for heavy fuel oil burners and igniters. The flue gas is pulled through the air heater and electrostatic precipitator with the use of two induced draft fans. Each of the ball and ring type coal (Babcock type 6.3E9) mills are charged with about 9-10 t.h⁻¹ of sub-bituminous type pulverized (pf) coal. The forced draft fans rated at about 60 m³.s⁻¹ flow rate supply the combustion air to the boiler. The main steam output gets distributed to pressure manifolds, of which customers are supplied with HP and IP steam. The overall process flow diagram (Figure 1b) of the boiler has been earlier reported in a separate study¹¹. Oil or gas fuels are generally used during the start-up of the boiler. The utility boiler did not have the steam air heater, steam reheaters, flue gas recirculation and circulating pump arrangements.

The fuel additive was stored in a silo away from the main boiler infrastructure and can be blown directly into the loss in weight feeder connected to the coal feeder feeding to the coal

mills. This injection method gives good control of mixing ratio between the pf and the fuel additive without causing downtime to the boiler. The fuel additive loss in weight feeder was set to feed in about 3.4% by volume or 6.8% by weight equivalent to the coal feed. The particle size distribution of the additive and UK-based utility coal along with proximate and ultimate analysis is shown in Table 1.

All the plant-related data operations have been controlled / logged by the Delta V control system. The collected samples of fly ash, bottom ash, pf coal, coal lumps from stockpile, coal mill rejects were analysed for ultimate, proximate, CV, loss on ignition (LOI), XRF and ash fusibility analyses, respectively. The thermal efficiency calculation for the boiler¹¹ was calculated as per the BS EN 12952-15:2003 standard (Eq. 1-4).

$$\eta (N)B = Q_N / Q_{(N)Ztot} \quad (1)$$

$$Q_N = m_{ST}(h_{ST} - h_{FW}) + m_{SS} (h_{FW} - h_{SS}) \quad (2)$$

$$Q_{(N) Ztot} = m_F H_{(N)tot} + Q_{(N)Z} \quad (3)$$

$$Q_{(N) Ztot} = m_F [(H_{(N)} + C_F(t_F - t_r)) / [1 - (\gamma_{Ash} (1 - v)) / (1 - \gamma_{Ash} - \gamma_{H2O}) ((u_{SL} / (1 - u_{SL})\eta_{SL} + (u_{FA} / (1 - u_{FA})\eta_{FA}))] + \mu_A C_{pA}(t_A - t_r)] + P_M + P \quad (4)$$

The calibration of the plant's continuous emission monitoring (CEM) analysers, collection of the fuel-fly/bottom ash-mill reject- fly ash samples, steady loads on the mill/boiler, water quality control was maintained during the test duration.

2.3. Corrosion test facility

The imperative effects of the additive technology are of major interest in the overall assessment by the industry. To this end, a number of studies were performed to determine the effects of deposits including the additive on corrosion rates. The corrosion test facility (Figure 1c) utilized for this study comprised of 6 silicon carbide electrically heated elements transversely placed in the top half of the furnace. The heating elements can modulate the temperature of the heated chamber up to 1200°C. A gas mixture skid supplied the humidified simulated combustion gas products (O₂: 3-4%, CO₂: 14-16%, HCl: 0.03-0.05%, SO₂: 0.13-0.15%, N₂: 75-78%, H₂O: 6-8%) inside the electrically heated chamber. The simulated gas mixture is supplied through a metered skid connected to dedicated gas bottle cylinders. Thermal mass flow controllers based on the heat conductivity of fluids are used to control and determine the mass flow. These thermal mass flow meters were calibrated by the supplier for the specific gas concentrations. A slight negative pressure differential of about 0.05-0.09 mbar was maintained across the heated chamber of the corrosion test facility by using a compressed air venturi vacuum generator, due to low flow rates. The exit flue gas mixture was scrubbed through a frequently replaced solution of NaOH (0.5mol).

T22 ferritic steel alloy (Cr: 2.25%, Mo: 1%) sample coupons after surface preparation²²⁻²³ and coating with the coal fly ash and fuel additive (Silanite™) mixed fly ash were placed inside the crucibles positioned in the heated compartment. The specimen coupons were all prepared in the same way by polishing to a uniform surface roughness using P120, P 240, P 280, P400 and P1200 silicon carbide paper for later dry polishing with diamond paste. 24 point measurements were taken across the whole surface of the polished coupons using a Mitutoyo +/- 2-micron accuracy micrometer to acquire an average thickness of coupons. Ethanol was added to the fly

ash to facilitate a uniform stable coat (ethanol would be dried off at room temperature). Uniform coatings were applied despite extra care for producing a uniform layer with consistent gram approximately 0.25% differences in the applied coating weight on duplicates was observed. These coupons were conditioned at 200°C [473.15K] in the furnace for 2 h after coating each specimen with the collected ash samples (Table 1). These coupons later were shifted to crucibles for weighing and positioned inside the furnace exposed to the simulated combustion environment maintained at 560°C [833.15K] for 1000 h. The coated coupons were placed on top of the ceramic plate and covered with an inverted ceramic liner with gas tight inlet and outlet connections. The heated compartment comprised of a base Inconel plate which is protected by a ceramic plate, the peripheries of Inconel plate were sealed with high-temperature grade silica powder.

The coupons were later analysed by accurate measurement for the metal loss. This was achieved by removing any deposited scale after 1000 h exposure to reach to the bare metal and again 24 point measurements at the same positions were taken to compare the difference in measurements between pre and post testing. These coupons were prepared in duplicates and the reported findings are based on the average of the results.

3. RESULTS AND DISCUSSION

The following section details the overall findings associated with the technology. The evaluated parameters alongside the discussions on array of tests performed on all of the aforementioned setups starts from the commercial to the pilot scale tests.

3.1. BS EN 12952-15:2003- full-scale boiler commercial test

A detailed breakdown of the test protocol followed during the test is shown in Table 2. The reported findings are associated with the full scale boiler test incorporating the overall impact on the efficiency, emissions, flame temperature, LOI, dust concentration, particle size distribution (PSD), slagging and fouling propensities and ash fusibility temperatures mainly at constant injection rate of the additive for 1 h and 7-8 h. The main range of varied parameter during the commercial scale boiler test was injection rates and mainly time of injection of the additive. The EN 12952-15 acceptance test criteria dictate for at least 4 h recommended duration of test with frequency of readings observed in a range from 3-15 mins. The 1 h trial test results were initially performed to confirm rate of injection of the additive and mill- boiler performance indicators. However the wider in depth effect of the 3.4% by vol. additive over a longer duration is explored in this paper.

3.1.1. The commercial full scale 8 h long test results on the 260 t.h^{-1} , as per the BS EN 12952-15: 2003 resulted in a net gain of about 1.05% increase in the boiler efficiency (Eq. 1-4, Table 3). An overall 7-8 h of steady state levels were maintained by keeping the loads on the coal mill- downstream high-intermediate pressure steam manifolds under unaltered conditions. The costs savings on the fuel input for maintained fixed output from the plant could also be regarded as an additional CO_2 reduction (due to reduced parasitic load on coal mills / air heaters and other ancillary equipment because of 1.05% less coal consumption).

3.1.2. A net 8.4% reduction in NO_x has been found compared to coal baseline with the addition of 3.4% by vol. (i.e. 6.8% wt.) fuel additive (Figure 2a). This NO_x reduction is in line with predictions (trials done earlier on $100 \text{ kW}_{\text{th}}$ pilot-scale combustion test facility and a 45 min trial on 280 t.h^{-1} steam-producing boiler¹¹ (Figure 2b-c). The CEM of NO_x emission (uncorrected) at the three different locations of the boiler for the baseline tests were reported as 195, 201 and 382

mg.Nm⁻³. They were compared at the same locations as 185, 167 and 357 mg.Nm⁻³ respectively when firing with 3.4% vol. additive injection. Then these measurements were corrected for the standard oxygen concentration of 6% (dry basis) along with plant recommended CEM instrument correction factors. The corrected NOx value for the baseline of 564 mg.Nm⁻³ was compared with NOx value obtained during the additive injection of 517 mg.Nm⁻³. The trial results have proven a net 8.4% reduction with the addition of 3.4% by vol. additive. This is in line with the earlier trials on both pilot and full-scale combustion test facility and boiler, respectively. CEMs normally get purged after every 12 h; hence around 14:10 the instruments got purged with air as evident from Figure 2a. The scatter of the points in the initial coal baseline when calculated as standard deviation was 21.60 compared to 25.57 for coal and coal with additive, respectively. Post additive injection, the downstream demand of the steam increased resulting in the increase of the coal mill loads (i.e. after 15:00). Hence the higher fuel to air ratio (i.e. fuel rich condition) produced lower NOx levels (Figure 2a).

3.1.3. The monitoring and characterisation of the coal / coal-additive flames on the viewing port of landing B of the boiler was also undertaken. The flame measurement was recorded for 8-10 minutes with the flame videos taken at a frame rate of 25 fps (frames per second) for observation purposes. The camera of the system was kept at the same settings (iris and exposure time) during the test. It was found that no detrimental effect on the flame temperature was recorded with the addition of the additive. In fact, 11°C [284.15K] increase in the average flame temperature (Figure 3a) was observed with the additive injections in comparison to coal baseline (1494°C) [1767.15K] unlike around 4 °C [277.15K] rise observed by the CC-88 additive based technology¹⁵. Each condition used to compute the average flame temperature included 150 to 200 simultaneous images. Temperature distribution of flames was computed using flame images

averaged over 20 simultaneous images based on the two colour method²⁴. Moreover, the power spectral density (PSD) of the flame signal (Figure 3c) were computed based on the average grey-level of each image from the video images recorded using the high speed mode (200 fps) of the camera over about 2 minutes²⁴. The oscillation frequency of the flame with and without additive was obtained using the weighted PSD of the flame signal. It remained in the range of 27-30Hz suggestive of no adverse effect of the additive on flame stability. The effect of the additive on the flame area was examined by applying an appropriate threshold to the segmented luminous region of each image; this was later normalized to the image size. These normalized flame areas were recorded to be in the range of 28% to 30% for coal and coal + Silanite™ baselines (Figure 3c), this seems to suggest that flame area was slightly more converged with the additive.

3.1.4. The fly ash samples were taken from the fly ash hoppers post Electrostatic precipitators (ESPs). The hoppers were emptied before and after steady state conditions by a dedicated fly ash recovery vacuum system, this allowed collection of the representative coal fly ash samples. The representative samples were stored in air tight clearly marked barrels for further analysis. Barrels numbered 1 to 11 were designated for coal fly ash collection; whereas barrels number 13 to 23 were used to collect fly ash with the additive. Later two more samples were taken post additive injection in Barrels 25-26. The collected samples were later analysed as per ASTM D7348 to determine the loss on ignition (LOI) values. The calculation of loss on ignition (Eq. 5) from the single step procedure used is as follows:

$$\text{LOI} = [(W-B)/W]*100 \quad (5)$$

Where W = mass of test specimen used, g, and B = mass of test specimen after heating at 950°C [1223.15 K], g. The LOI values for coal fly ash samples gave a range from 14.5% to 15.7% for

barrels 1 to 11. This averages to be about 15% -coal fly ash baseline. On the other hand, a range of 8.1% to 9.8% was determined for coal + 6.8% Silanite™ fly ash samples, averaging to be about 8.6%. Figure 4 shows the LOI data points respective to samples collected from 1st, 2nd or 3rd fly ash hoppers post ESPs. The scatter of the points in the initial coal baseline when calculated as standard deviation was 2.8 compared to 3 for coal + 6.8% Silanite™. A net 42.7% reduction in LOI was observed with the injection of the fuel additive. In all cases, LOI in fly ash show the reduction after injecting the fuel additive. In refs 10.56% reduction in the carbon in ash¹⁵ and improvement in the color of fly ash has been reported¹⁶ unlike around 43% reduction in carbon with Silanite™ additive.

3.1.5. Dust concentration post electrostatic precipitator (Figure 5) has been reduced by approximately 18% with the Silanite™ injection indicating better performance of ESPs. The reductions in the unburned carbon present in the fly ash and the conductive properties of the oxides of iron (in the additive) have resulted in the reduction of dust concentration emitted in the stack. Silanite™ injection delivers a positive impact on the chemical composition of fly ash, particle size and the resistivity- crucial parameters for improvement of the electrostatic precipitator performance. The recorded concentration of the dust post ESPs are tabulated in Table 4 and Figure 5 entails dust concentration plots for 45 min- 8 h and 1 h trials carried out on the same boiler along with the full-scale BS EN 12952 8 h test. The scatter of the points in the initial coal baseline when calculated as standard deviation was again close to that of coal with Silanite™. Other competing studies^{16, 18} make qualitative claim of increase in the ESP performance and reduction of fly ash resistance. However, it is difficult to compare the results of other qualitative claims with quantified results of this study.

3.1.6. The Air Jet PSD analysis conducted on the coal – Silanite™ fly ash samples collected during the 8h trial indicated 90% passing at 335 microns compared to 508 microns for the coal fly ash. It is also evident from Figure 6 that the coal + additive mixed fly ash is finer than compared to coal fly ash. This is mainly associated with the injection of the additive having d0.9 less than 34 microns compared to a typical coal having d0.9 less than 125microns. The fineness of the coal - Silanite™ fly ash also qualifies it for EN450 (not more than 40% retained on the 45 microns sieve). The resultant coal fly ash with the injected Silanite™ is finer than coal fly ash.

3.1.7. The slagging and fouling propensities calculations from the full scale 8 h trial have indicated no detrimental impact on the slagging and fouling propensities. This is due to the combined concentration of the oxides of iron, aluminium and silica. Table 5 entails the findings of XRF analysis with the major and minor elemental oxide concentrations present in the fly ash and Silanite™ respectively. These concentrations have been utilised to calculate the fouling and slagging indices as per the Eq.6-7.

$$\text{Fouling Indices}^{25-26} = Fu = (B/A)(Na_2O + K_2O) \quad (6)$$

$$\text{Slagging Indices}^{25-26} = Rs = (B/A)S^d \quad (7)$$

where $(B/A) = (Fe_2O_3 + CaO + MgO + Na_2O + K_2O) / (SiO_2 + Al_2O_3 + TiO_2)$ in dry fuel

3.1.8. The samples collected as part of the 8h trial were subjected to ash fusibility as per BS ISO 540:2008. The ash fusibility temperatures were determined using Carbolite digital CAF-8. The samples tested were analysed on an as received basis. Ash samples were mixed with an adhesive dextrin solution to prepare a paste mixture. The cylindrical mould was first coated with a thin layer of petroleum jelly. The mould was uniformly and completely filled with the prepared

paste of ash so that edges of cylindrical test pieces are sharp. Upon visual drying, the specimens are removed from the mould on its support to dry overnight. Two identical cylindrical samples were prepared for the same sample for repeatability purposes and placed on support next to each other. The test pieces were visually examined with the camera after loading in Carbolite digital furnace. The slow gradual increase in temperature @ 10 °C/min [283.15K/min] to about 815°C [1088.15K] caused the removal of any organic matter. The specimen and recording of the shapes at intervals of temperature change not greater than 10 °C [283.15 K] were recorded until the flow temperature of the specimen was attained. The fusibility temperatures observed during the analysis are defined as follows; the deformation temperature at which the first sign of rounding, due to melting, of the tip or edges of the test piece, occur. Sphere temperature is at which the edges of the test pieces become completely round with the height remaining unchanged. Hemisphere temperature at which test piece forms approximately a hemisphere (height becomes equal to half of the base diameter). Flow temperature at which the ash melt spread out over the supporting tile in layer (height of which is one-third of the height of the test piece at the hemisphere temperature). The analysis of the samples did not indicate a difference in the initial deformation and sphere temperatures of coal fly ash samples with and without additive, however, hemisphere and flow temperatures were observed to be higher for coal- Silanite™ fly ash compared to the simple coal fly ash (Table 6). This is an indication of the formation of high temperature eutectic mixtures of fly ash with the lower slagging propensity. It is evident from the data that a suppression of about 10°C-30°C was observed in the flow temperature with the additive combined coal fly ash samples. Similarly a 10°C-20°C [283.15K- 293.15K] increase in hemisphere temperature was observed for additive combined coal fly ash samples.

Injection of silica based additive¹⁴ to lignite coal fired industrial boiler also inhibit the slagging and fouling due to scavenging of highly molten slag by added silica. The stable Fe⁺³- silicate formations due to high melting points and viscosity also contribute to inhibition of slagging¹⁴. Silanite™ additive originally containing both magnetite and fayalite phases resulted in promotion of magnetite formation proven by the ash collected from the convective sections of the boiler¹¹. This formation could be partially based on the mechanism proposed for iron speciation by ref¹⁴.

During the ash fusibility tests it was also verified that the coal fly ash samples exhibited greater shrinkage rate compared to the Silanite™ -coal fly ash samples. The shrinkage of the samples with temperature can be observed in a sequential comparison of the images obtained. The image analysis has revealed that there was an overall 53.26% reduction in the image area of coal fly ash sample compared to 46% reduction in the image area for coal with the additive fly ash sample. The approach has been applied to other samples endorsing relatively lesser shrinkage compared to the simple coal fly ash samples. These remarkable differences of shrinkage rates are attributed to sintering characterisation of the fly ash. Hence from the analysis of the images, it has been shown that coal with additive fly ashes has relatively lesser tendency to sinter compared to the simple coal fly ash because of lesser shrinkage rates.

3.2. 100kW_{th} furnace test results

The reduction of NO by combustion intermediate i.e. CO over the surface of oxides of iron^{11-12, 27-29} was validated by the recorded radial and axial profile measurements from the pilot scale 100kW_{th} furnace combustion tests at 15% excess air for 3.4% by vol. addition of the additive. Convincing evidence specifies better results towards de-NOx using iron oxides in

conjunction with other commercially available technologies i.e. reburning, advance reburning, selective non-catalytic reduction²⁹⁻³¹. The inflame measurement of CO at the module 1 (port 1) position confirmed higher concentrations with Silanite™ (Figure 8a) compared to coal baseline measurement at the same location. However, later at the module 2 (port 2) location, the values were recorded lower than the respective coal baseline measurements. An increase in the production of the lighter hydrocarbon (i.e. CO) from the coal matrix due to the possible exothermic reactions¹², pyrolytic cracking³² and increased surface area and pore structure³³, in the near-burner zone is visible from the first set of radial profile measurements at module 1. However, a shift can be seen as the reactions carry forward in the later part of stationary combustion source (module 2, port 2 position) where the concentration of CO starts to reduce in order to facilitate the self-reduction of oxide phases of iron with non-conjectural NOx reduction (Figure 8a). This has been discussed to be linked with the oxides of iron / iron as a gas phase catalyst or as indirect heterogeneous NOx reduction catalyst²⁷. There is also evidence associated with the iron metal cations in the ion-exchanged forms, present in coal or coal ash, changing the ratio of heavy hydrocarbon to lighter hydrocarbon²⁹. The in-furnace reduction of NO achieved without the need of an additional reactor has been reported in literature^{27, 29} not only under fuel rich but equivalently in fuel lean conditions.

It can be inferred from the traverse profiles (Figure 8a) that the test facility burner flame is not exactly symmetrical from the center axis of the burner, due to heterogeneous combustion characteristics of coal. The traverse measurement was taken over a 15 mins with frequency of readings recorded after 10 s for both with and without additive injected conditions. The error bars are shown in Figure 8a, also taking into account the 95% accuracy confidence of the data based on the standard deviation. The O₂ trends for the module 1 (port 1) position are relatively at

lower level values compared to the module 2 (port 2) positions, indicative of the extension of fuel-rich combustion zone from the burner quarl up till module 1 position. Figure 8b also indicates a shift from the fuel rich zone to fuel lean zone while moving axially down to the flue emission point. A net 8.2% NO reduction was achieved with 3.5 vol. % Silanite™ injection. It has been reported that the surface to surface based reactions are mainly responsible for the solid iron based additives; however, the gas species might also play a role towards NO destruction in fuel rich zones²⁷. Even though the iron oxide chemical redox reactions have a negative Gibbs free energy, the NO destruction would still converge to a limit (optimum value) as the mass fraction of the additive is increased.

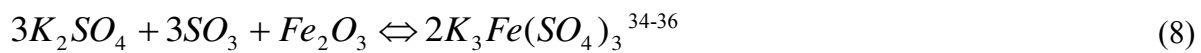
The collected fly ash from the pilot scale facility was subjected to analysis using the scanning electron microscope with energy dispersive spectroscopy. Table 7 summarizes the overall spectrum with 5 iterations of the metal % present in the fly ash samples with and without the additive. It is shown that based on the spectrum analysis the metal concentration of iron in the fly ash increased by about twofold. The results show the net reduction in the K% which is beneficial to suppress the potassium based corrosion sulphidation reactions. The previous tests¹¹ have shown the formation of the magnetite phase due to the possible interaction of fayalite and CO₂. Moreover, the presence of Fe₂O₃ at 1100°C [1373.15K] with the potential formation of magnetite at about 700°C has also been reported by other researchers^{29-30,34}.

3.3. Corrosion test results

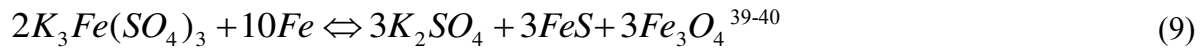
In an industrial application, fireside corrosion poses a vital challenge so as to reduce the downtime required to repair failed superheater (SH) and reheat (RH) section boiler tubes. In order to examine the effect of Silanite™ on alloy specimen T22 (widely used for SH and RH

boiler section tubes) was tested under simulated flue gas concentration. Figure 9 presents the mass gain and rate of corrosion of the alloy T22 specimens after 1000h exposure at 570°C [843.15K], coated with coal and Silanite-coal fly ash collected from both the 100 kW_{th} and commercial boiler (260 t.h⁻¹ steam production rate).

The Silanite-coal fly ash-coated T22 alloy presented reduced corrosion rates (Figure 9b) compared to the simple coal fly ash-coated and non-coated specimens. The total amount of alkali oxides reported in Table 1, especially the volatile oxides (Na₂O, K₂O) of the collected Silanite™ + Coal fly ash sample (used for coating purposes) is lower than coal fly ash. This has a direct impact on the known reactions associated with the transformation of alkali chlorides to form alkali sulphates (K₂SO₄) reacting with the oxides of iron (Fe₂O₃) and SO₃, eventually resulting in the formation of alkali iron trisulphates³⁵⁻³⁷. This compound known for its lower melting point dependent fluidity could enhance the rate of corrosion³⁵ and the steps involved are pictorially explained in Figure 10. The triggering alkali oxides at high temperature react with the water vapours of the surrounding simulating gas mixture to form alkali hydroxide (KOH, NaOH) which after reacting with SO₃ form alkali sulphate (*K₂SO₄, Na₂SO₄*) deposits. Moreover, the continuous formation of these sulphates allows the diffused oxygen to the metal scale of the specimen to form trioxide of iron (Fe₂O₃) which reacts with SO₃ to form iron sulphates (Fe₂(SO₄)₃). The already formed K₂SO₄ would then react with Fe₂(SO₄)₃ to form the molten layer of low melting alkali iron trisulphates³⁵⁻³⁷. Eq. 8 summarises these reactions with a rate dependent on the concentration of sulphates of the oxides of alkali.

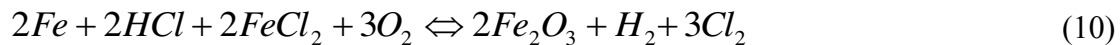


The primitive deposits associated with the sulphate; K_2SO_4 , Na_2SO_4 have melting points³⁹ of 1067°C [1340.15K], 888°C [1161.15K] respectively. However, the thermal stability limit of the alkali iron trisulphates is around 570°C - 590°C [843.15K- 863.15K]^{37,39}. This unstable molten compound reacts with the base metal of the T22 alloy as per the Eq. 9 resulting in the loss of the boiler tube wall thickness.

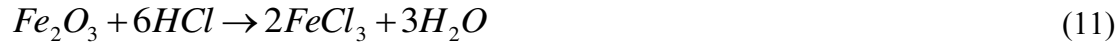


The formation of the alkali molten complex progresses (Eq. 9) in the form of a continuous reaction cycle³⁹⁻⁴⁰ based on the formation of the K_2SO_4 (Eq. 8). In the present study due to the presence of relatively lower concentration of oxides of potassium in the Silanite™ + Coal fly ash samples (both 100 kW_{th} and 260 t.h⁻¹ steam producing boiler), the formation of these alkali molten complexes would be lower resulting in the evident reduced corrosion rates compared to the coal fly ash samples.

In relation to high temperature, chlorine based fireside corrosion, the direct attack of HCl present in the combustion gaseous products results in $FeCl_2$ formation, which upon oxidation produces Cl_2 able to penetrate directly to the metal resulting in a phenomenon called “metal chlorination at the metal surface”⁴¹ (Eq. 10⁴²⁻⁴³).



In the presence of the higher concentration of Fe_2O_3 (Table 1) in the Silanite™ + coal fly ash samples, a protective coating layer could potentially act as a barrier stopping the direct contact of HCl with the base metal (Eq. 11). The iron oxide would then react with the HCl / Cl_2 at the deposit coated surface before they could diffuse into the base metal.



Moreover, the formation of Chromia (Cr_2O_3 - present in the Silanite™ + coal fly ash) approximately twice compared to the coal fly ash could (Table 1) can act as a very protective layer preventing the iron-rich oxides formation of the iron from the base metal⁴³. The above explained mechanisms in the presence of the additive can be summarized as follows: lower alkali oxides and higher oxides of iron concentrations in the deposit formations are expected to lead to a lower corrosion rate.

Figure 9a show that the Silanite™ additive mostly increased the weight gain of the samples, and that the T22 alloy without any coating had the highest weight gain. The pure T22 alloy without any coating due to the direct exposure to the simulated flue gas concentration produced oxidative layers of the oxides of the base metal. The SEM/EDS results of the cross-sectional view of the corroded T22 specimen without any coating (Figure 11a) only indicated rich in Fe, O₂ and Cr in the intact oxide scale compared to only Fe, Cr and Mo of the base metal. Due to the high presence of Fe and O (Fe_2O_3) along with Cr, the iron oxide can then form a thick layer of $FeCr_2O_4$ (chromium / iron compound spinel) as evident from the EDS of Figure 11a. Similarly, with the presence of additional iron oxide of Silanite™ + Coal fly ash and twice the amount of Chromia (Cr_2O_3), the formation of the same complex Fe/Cr spinel can add to the overall weight gain (Figure 11c). The molar mass of $FeCr_2O_4$ i.e. 223.8 g/mol is also relatively higher compared to the molar mass of oxide of iron i.e. Fe_2O_3 : 159 g/mol. In case of the observed findings with the Silanite™ + Coal fly ash coatings, the weight gain due to Fe/Cr spinel formation could exceed the decrease in the weight gain due to the lower corrosion rate. Therefore, in the Figure 9b, an overall weight gain in case of Silanite™+Coal fly ash has been observed. The lower concentration of O (35.8%) in the mapped box (Figure 11c) of the

simulated flue gas exposed Silanite™+Coal fly ash coating, compared to the O (52.3%) (Figure 11b) of the Coal fly ash coating especially with lower K (0.3% instead of 0.9%) supports the presence of a lower concentration of the low melting complexes compared to $2K_3Fe(SO_4)_3$. It is also interesting to observe that the thickness of the scale formation due to corrosion above the base metal is slightly thicker in case of the T22 alloy with and without coal fly ash coating (Figure 11a-b), compared to the Silanite™+ Coal fly ash coating (Figure 11c).

The average surface area of each of the specimen coupons is approximately 1.5cm^2 , the mass density gain of the studied samples ($\text{g}\cdot\text{cm}^{-2}$) are as follows: T22 without coating = 16.67, T22 Coal fly ash from the 100kW_{th} CTF = 10.23, T22 Silanite+ Coal fly ash from the 100kW_{th} CTF = 10.47, T22 Coal fly ash from the 233MW_{th} boiler = 5.6 and T22 Silanite™+Coal fly ash from the 233MW_{th} boiler = 11.37. A similar study⁴⁴ on T22 alloy with different coatings produced a higher density gain of $45\text{g}\cdot\text{cm}^{-2}$ due to the wide difference between the alkali oxide / sulphates concentrations though with the similar iron oxide concentration.

Other competing technologies¹⁵⁻¹⁹ report corrosion reduction by means of the additives, however, the impact with Silanite™ additive is analysed whether it is significant enough to improve the life span of the real power plant boiler tubes. In the present study with 2.25% Cr ferritic steel tubes the minimum and maximum corrosion rates (mm/year) of approximately 0.345 and 0.352 was achieved with Silanite™+Coal fly ash coatings produced from both the pilot and commercial tests. Usually 33% of the thickness is the limit for corrosion in the boiler tubes, which for a typical 38mm diameter superheater tubes is about 1.51mm^{45} . The life span of the boiler tubes due to coating can be assumed to be reasonably estimated from the achieved corrosion rates. Therefore the life span of the corrosion deposit without additive coating will approximately be $1.51/0.468$ which equals an estimated value of 3.2 years; whilst the corrosion

with additive coating will have a life span of $1.51/0.352$ which equals an estimate of 4.2 years. This investigation reveals that the Silanite™ additive is capable of increasing the life span of a high temperature super-heater tubes by approximately 1 year.

4. CONCLUSIONS

The technology demonstrated on 233 MWth (260-280 t.h⁻¹ steam output) pulverized fuel boiler a net 42% reduction in LOI, 20% decrease in the particulate matter of ESP, 8% NO_x reduction with 11°C increase in the flame front for 3.5 vol. % injected additive. The iron oxide chemical redox reaction verified by the radial and axial profile measurements from the pilot scale are responsible for NO destruction along with production of lighter hydrocarbon. The 1000 h corrosion rate findings on T22 tube sections exposed to 833.15K indicate an increase in the lifespan of boiler tubes from 3.2 to 4.2 years due to the following reasons:

- 1) Lower concentration of oxides of potassium in the additive coating reduce the continuous reaction cycle of low melting iron trisulphates complexes formations.
- 2) Additive coating with built in iron oxide layer acts as a barrier to inhibit the direct metal chlorination.
- 3) Presence of Chromia (Cr₂O₃ in the additive) acts as a protective layer preventing the oxidation of the base metal.

ACKNOWLEDGMENTS

Additive base technology is patented by International Innovative Technologies UK (IIT) UK Ltd GB (GB 2516728). The support of the analytical team at IIT Ltd and the independent

body of due diligence experts to monitor the commercial full scale boiler tests are highly appreciated. Authors would also like to thank Mr. Scott Taylor for his in valuable industrial test site support and all other involved research groups. The support from post graduate student (Tom Yelland) and experimental officers (Dr Cheryl Shaw, Dr Peng Zeng, Mr. Michael Bell) at University of Sheffield is highly commended. The project has been partly funded by the TSB through KTP-008393 and the corrosion results have been funded under the innovation agreement industrial grant (IIT Ltd).

NOMENCLATURE

m_{ST} = Main steam flow, kg.s^{-1}

h_{ST} = Specific enthalpy of main steam, kJ.kg^{-1}

m_{SS} = Spray water flow rate to the main steam at temperature, kg.s^{-1}

h_{SS} = Specific enthalpy of spray water, kJ.kg^{-1}

h_{FW} = Specific enthalpy of spray water, kJ.kg^{-1}

m_F = Total coal flow to the boiler, kg.s^{-1}

$H_{(N)tot}$ = Net total calorific value of the coal, kJ.kg^{-1}

C_F = Specific heat of the fuel, $\text{kJ.kg}^{-1}.\text{°C}^{-1}$

t_F = Average temperature of the coal supply (fuel), °C

t_r = Reference temperature, °C

C_{PA} = Specific heat of the air, $\text{kJ.kg}^{-1}.\text{°C}^{-1}$

μ_A = Combustion air to mass fuel ratio, kg.kg^{-1}

γ_{Ash} = Ash content in the fuel, kg.kg^{-1}

γ_{H2O} = Moisture content in the fuel, kg.kg^{-1}

v = Volatile matter content of ash, kg.kg^{-1}

u_{SL} = Unburned combustible content of slag, kg.kg^{-1}

$\eta_{SL} = 0.05$ = Ratio of collected furnace bottom-ash mass to mass of ash in fuel minus its volatile fraction

u_{FA} = Unburned combustible content of fly ash, kg.kg^{-1}

η_{FA} = 0.95 = Fly ash retention efficiency

P_M = Coal Pulveriser power, kW

P = Any other power required on motors, kW

Q_N = Useful heat output, kW

$Q_{(N)Ztot}$ = Total heat input, kW

$\eta(N)B$ = Thermal efficiency by Direct method

REFERENCES

- (1) World Nuclear Association website; <http://www.world-nuclear.org/information-library/energy-and-the-environment/renewable-energy-and-electricity.aspx>.
- (2) World Coal Association website;
http://www.worldcoal.org/file_validate.php?file=Coal%20Facts%202015.pdf.
- (3) Ouyang, Z.; Zhu, J.G.; Lu, Q.G.; Yao, Y; Liu, J.Z. The effect of limestone on SO_2 and NO_x emissions of pulverized coal combustion preheated by circulating fluidized bed. *Fuel* **2014**, *120*, 116–121.
- (4) Qin, L.; Zhang, Y.; Jan, J.; Chen, W. Influences of waste iron residue on combustion efficiency and polycyclic aromatic hydrocarbons release during coal catalytic combustion. *Aerosol and Air Quality Research* **2015**, *15*, 2720-2729.
- (5) Technical report on PentoMag® 2550 anti-slagging coal additive. Accessed on 12.02.2016. <http://www.pentol.com/sites/default/files/pentomag2550-techinfo.pdf>

- (6) Mortson, M.; Xia, Q. Advanced pollution control-the airborne process and its benefits to china. Accessed on 12.02.2016. http://www.airbornecleanenergy.com/uploads/3/8/7/6/38765463/paper_for_china_conference.pdf
- (7) Gong, X.Z.; Guo, Z.C.; Wang, Z. Variation on anthracite combustion efficiency with CeO₂ and Fe₂O₃ addition by differential thermal analysis (DTA). *Energy* **2010**, *35*, 506–511.
- (8) Mendiara, T.; Diego, L.F.; Labiano, F.; Gayán, P.; Abad, A.; Adánez, J. On the use of a highly reactive iron ore in chemical looping combustion of different coals. *Fuel* **2014**, *126*, 239–249.
- (9) Zhang, S.; Chen, Z.; Chen, X.; Gong, X. Effects of ash/K₂CO₃/Fe₂O₃ on ignition temperature and combustion rate of demineralized anthracite. *J. Fuel Chem. Technol.* **2014**, *42*, 166–174.
- (10) Zou, C.; Wen, L.; Zhang, S.F.; Bai, C.G.; Yin, G.L. Evaluation of catalytic combustion of pulverized coal for use in pulverized coal injection (PCI) and its influence on properties of unburnt chars. *Fuel Process. Technol.* **2014**, *119*, 136–145.
- (11) Daood, S.S; Ord, G.; Wilkinson, T.; Nimmo, W. Fuel additive technology- NOx reduction, combustion efficiency and fly ash improvement for coal fired power stations. *Fuel*, **2014**, *134*, 293-306.

- (12) Daood, S.S; Ord, G.; Wilkinson, T.; Nimmo, W. Investigation of the influence of metallic fuel improvers on coal combustion / pyrolysis. *Energy and Fuels*, **2014**, *28*, 1515-1523.
- (13) Wang, L.; Hustad, J.E.; Skreiberg, O.; Skjevraak, G.; Gronli, M. A critical review on additives to reduce ash related operation problems in biomass combustion applications. *Energy Procedia*, **2012**, *20*, 20-29.
- (14) Dai, B.; Wu, X.; Girolamo, A.D.; Cashion, J.; Zhang, L. Inhibition of lignite ash slagging and fouling upon the use of a silica-based additive in an industrial pulverised coal-fired boiler: Part 2- Speciation of iron in ash deposits and separation of magnetite and ferrite. *Fuel*, **2015**, *139*, 733-745.
- (15) Yanjie, R. The result and analysis of CC-88 on boiler 6 at HCMI power plant. http://www.coaladditives.com/assets/documents/HCMItest_result.pdf.
- (16) Tellabus Trial report for Pentomag 2550 I – Coal additive. http://www.pentol.net/sites/default/files/pentomag2550-trial_naachiar-india.pdf.
- (17) Mortson, M.; Xia, Q. Advanced Pollution Control- the Airborne Process™ and its benefits to China. Airborne Clean Energy. http://www.airbornecleanenergy.com/uploads/3/8/7/6/38765463/paper_for_china_conference.pdf.
- (18) Pentol flue gas conditioning system- SO₃ injection for ESP optimization. <http://www.pentol.net/water-in-oil-emulsion/flue-gas-conditioning>.

- (19) Laird, C.P.; Smith, K.J.; Looney B. Results of the Dry Sorbent Injection testing to reduce HCl. <http://www.carmeusena.com/sites/default/files/brochures/flue-gas-treatment/tp-mega-symp-paper107.pdf>.
- (20) Glushkov, D.O.; Lyrshchikov, S.Y.; Shevyrev, S.A.; Strizhak, P.A. Burning properties of slurry based on coal and oil processing waste. *Energy and Fuels*, **2016**, *30*, 3441-3450.
- (21) Daood, S.S.; Javed, M.T.; Rizvi, A.H.; Nimmo, W. Combustion of Pakistani Lignite (thar coal) in a pilot-scale pulverized fuel down-fired combustion test facility. *Energy and Fuels*, **2014**, *28*, 1541-1547.
- (22) Hussain, T; Simms, N.J.; Nicholl, J.R; Oakey, J.E. Fireside corrosion degradation of HVOF thermal sprayed FeCrAl coating at 700-800°C. *Surface and Coating Technology*, **2015**, *268*, 165-172.
- (23) Rizvi, T. Fireside corrosion in oxy-fuel environments and the influence of fuel and ash characteristics on corrosion and deposition. Ph.D. Dissertation, University of Leeds, **2014**.
- (24) D. Sun, G. Lu, H. Zhou, and Y. Yan, 'Flame stability monitoring and characterisation through digital imaging and spectral analysis', *Meas. Sci. and Tech.*, 2011, *22*, 114009 (9p), doi:10.1088/0957-0233/22/11/114007.
- (25) Kazagic, A.; Smajevic, I. Experimental investigation of ash behaviour and emissions during combustion of Bosnian coal and biomass. *Energy*, **2007**, *32*, 2006-2016.

- (26) Masia, A.A.T.; Buhre, B.J.; Gupta, R.P.; Wall, T.F. Characterising ash of biomass and waste. *Fuel Processing Technology*, **2007**, 88, 1071-1081.
- (27) Lissianski, V.V.; Maly, P.M.; Zamansky, V.M. Utilization of iron additives for advance control of NO_x emissions from stationary combustion sources. *Ind. Eng. Chem. Res*, **2001**, 40, 3287-3293.
- (28) Gradon, B.; Lasek, J. Investigations of the reduction of NO to N₂ by reaction with Fe. *Fuel*, **2010**, 89, 3505-3509.
- (29) Lasek, J. Investigation of the reduction of NO to N₂ by reaction with Fe under fuel-rich and oxidative atmosphere. *Heat Mass Transfer*, **2014**, 50, 933-943.
- (30) Fennell, P.S.; Hayhurst, A.N. The kinetics of the reduction of NO to N₂ by reaction with particles of Fe. *Proc. Combust. Inst*, **2002**, 29, 2179-2185.
- (31) Su, Y.; Deng, W.; Shen, H. Catalysis reduction of NO and HCN/ NH₃ during reburning: a short review. **2012**, *Adv Mat Res*, 354–355:365–368.
- (32) Nozomu, S.; Nobuta, K.; Kimura, T.; Hosokai, S.; Hayashi, J.; Tago, T.; Masuda, T. Production of chemicals by cracking pyrolytic tar from Loy Yang coal over iron oxide catalyst in a steam atmosphere. *Fuel Processing Technology*, **2011**, 92, 771-775.
- (33) Noichi, H.; Uddin, A.; Sasaoka, E. Steam reforming of naphthalene as model biomass tar over iron-aluminum and iron-zirconium oxide catalyst catalysts. *Fuel Processing Technology*, **2010**, 91, 1609-1616.

- (34) Lasek, J.; Gradon', B. Możliwość wykorzystania żelaza i jego związków w niektórych działaniach na rzecz ochrony środowiska. *Hutnik- Wiadomości Hutnicze*, **2009**, 76, 813–819.
- (35) Reid, W.T. *External Corrosion and Deposits: boilers and gas turbines*, American Elsevier, New York, 1971.
- (36) Tomeczek, J. Corrosion modelling of austenitic steel in molten sulphate deposit. *Corrosion Science*, **2007**, 49, 1862-1868.
- (37) Nelson, W.; Cain, C.J. Corrosion of Superheaters and Reheaters of Pulverized-Coal- Fired Boilers. *Transaction of the ASME*, **1960**, 194-201.
- (38) Science lab Website; <https://www.sciencelab.com/msdsList.php>.
- (39) Spliethoff, H. *Power Generation from Solid Fuels*, Springer- Verlag Berlin Heidelberg: Berlin, Germany, 2010.
- (40) Ishigai, S. *Steam Power Engineering*. Press Syndicate of the University of Cambridge: Cambridge, UK, 1999.
- (41) Gaus-Liu, Xiaoyang. *High-Temperature Chlorine Corrosion during Co-Utilisation of Coal with Biomass or Waste*, Institut für Verfahrenstechnik und Dampfkesselwesen der Universität Stuttgart: Germany, 2008.
- (42) Grabke, H.K.; Reese, E.; Spiegel, M. The effects of chlorides, hydrogen chloride, and sulfur dioxide in the oxidation of steels below deposits. *Corrosion Science*, **37**, 1023-1043.

- (43) Chandra, K.; Kranzmann, A.; Neumann, R.C.; Oder, G.; Rizzo, F. High Temperature Oxidation Behavior of 9-12% Cr Ferritic / Martensitic Steels in a Simulated Dry Oxyfuel Environment. *Oxid Met*, **2015**, 83, 291-316.
- (44) Dudziak, T.; Hussain, T.; Simms, N.J.; Syed A.U.; Oakey, J.E. Fireside corrosion degradation of ferritic alloys at 600°C in oxy-fired conditions. *Corrosion Science*, **2014**, 79, 184-191.
- (45) Mujibur Rahman, M.; Kadir, A.K. Failure analysis of high temperature superheater tube (HTS) of a pulverised coal-fired power station. *Proceedings of Intl. Conf. on Advance Science*, **2011**, 517-522.

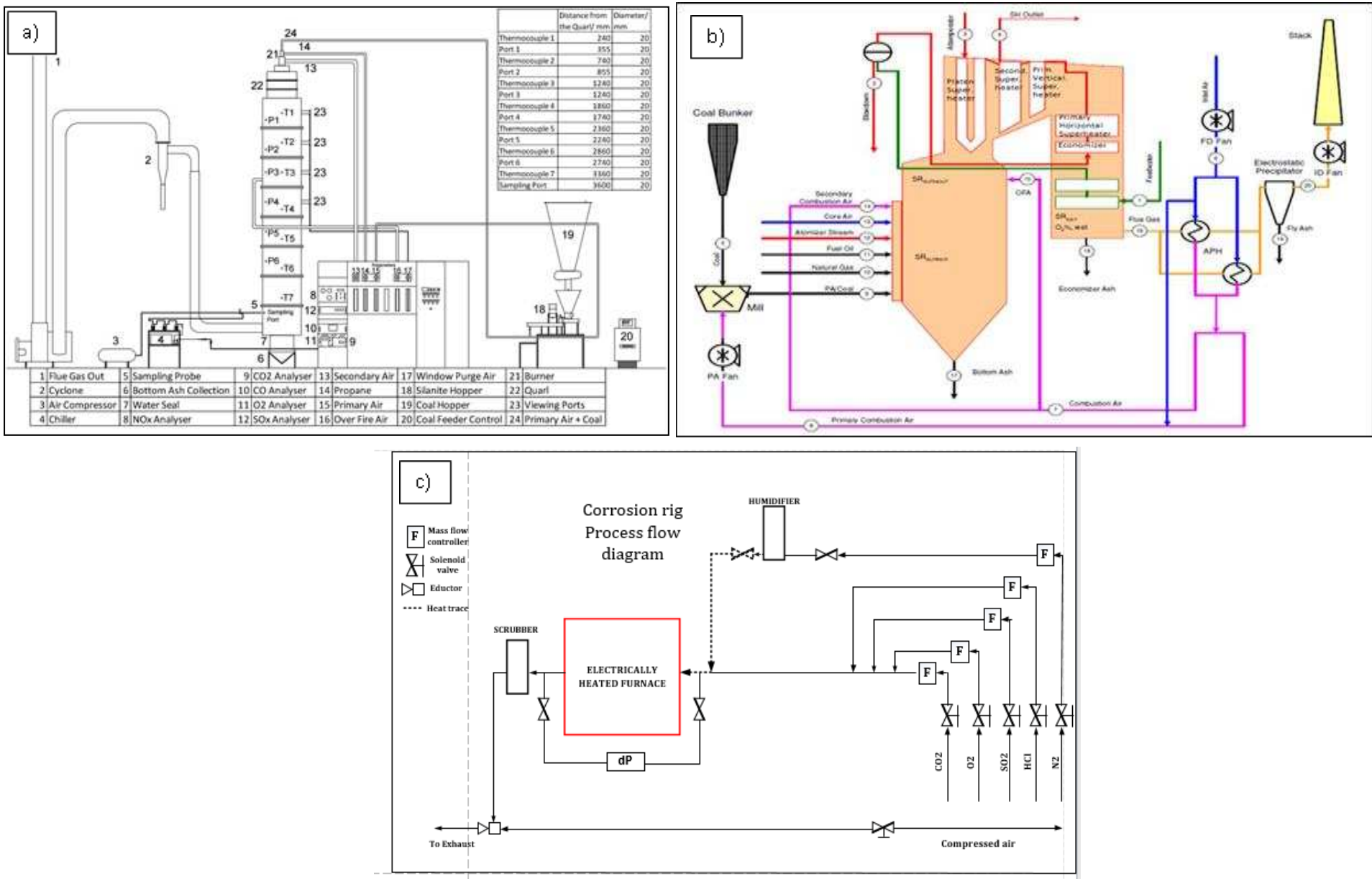


Figure 1. Equipment and schematics of the test facilities: a) 100kW_{th} combustion test facility, b) $260\text{t}\cdot\text{h}^{-1}$ steam producing commercial boiler [12], c) simplified schematic of the corrosion test facility.

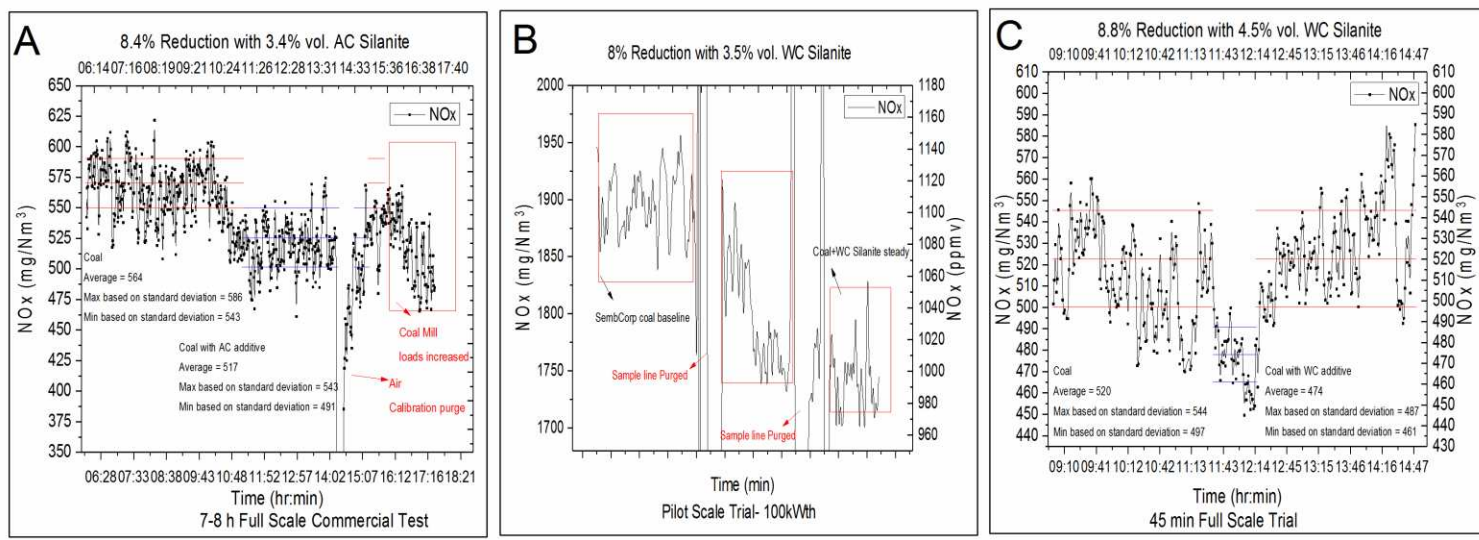


Figure 2. a) NOx profile 8h full Scale Commercial Test; b) Pilot Scale Trial- 100 kW_{th}; c) NOx profile 45 min Full Scale Trial [12].

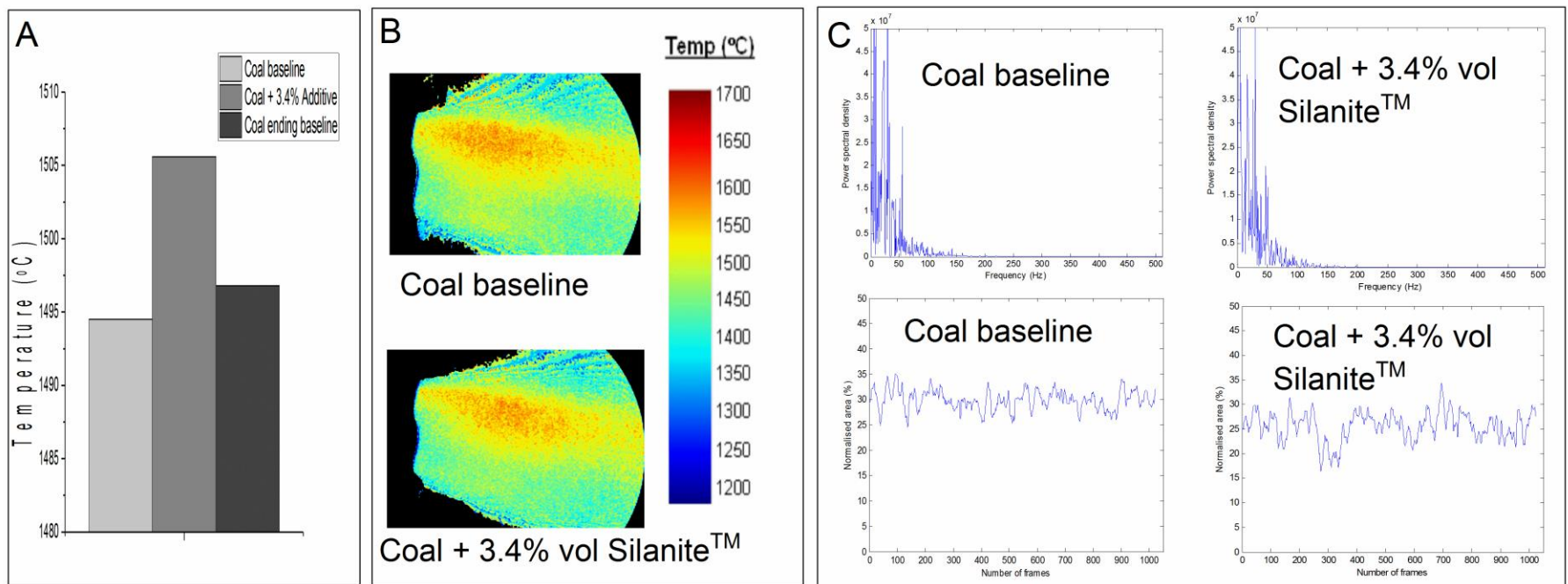


Figure 3. Effect of the injection of Silanite™ on the flame temperature, oscillation frequency and flame area

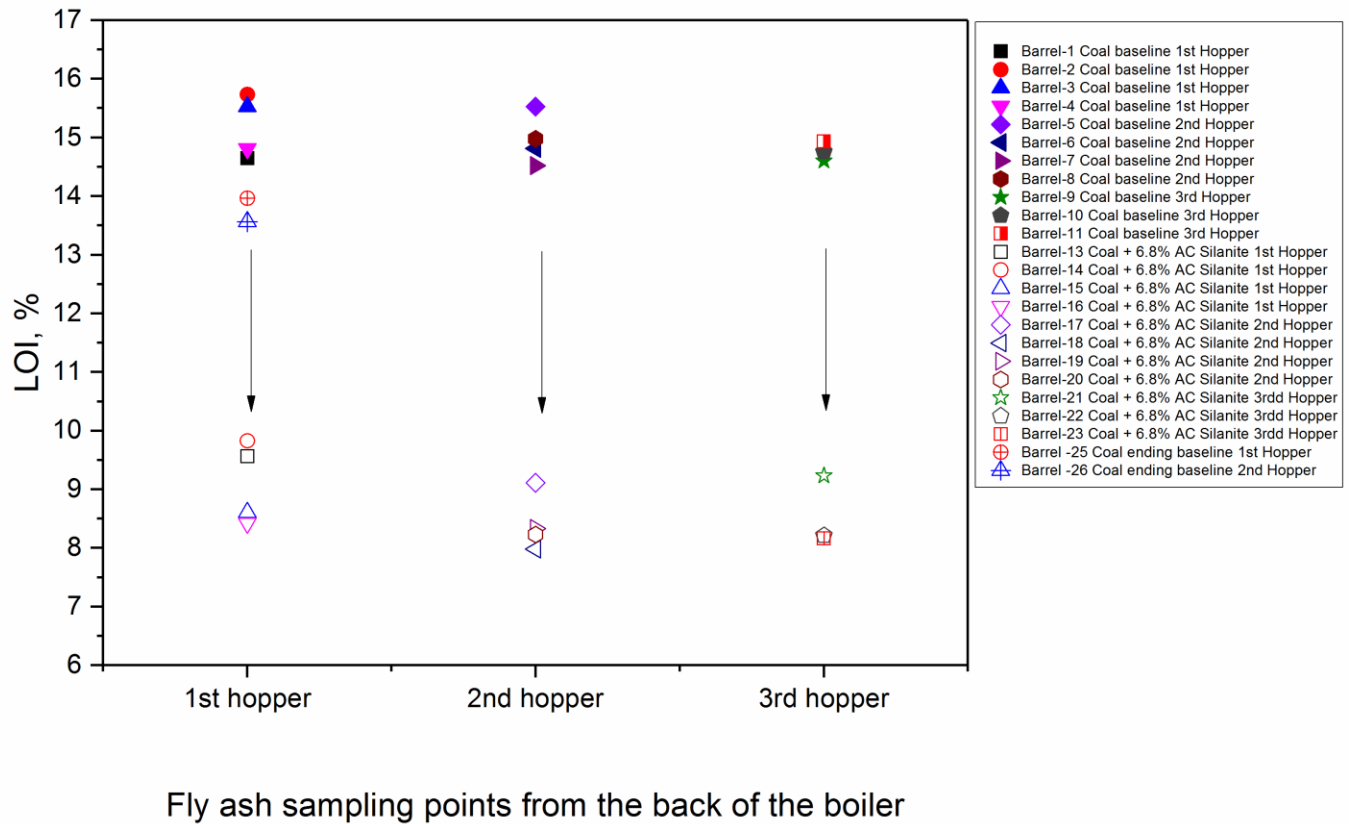
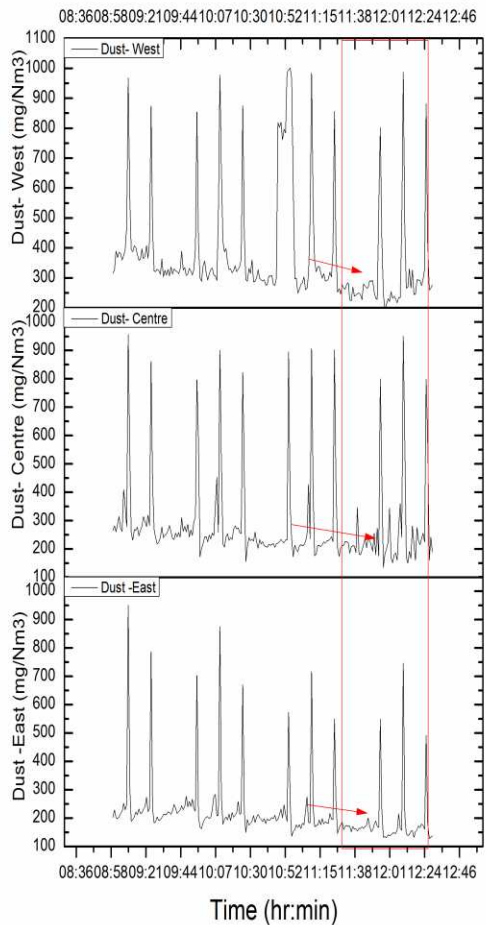


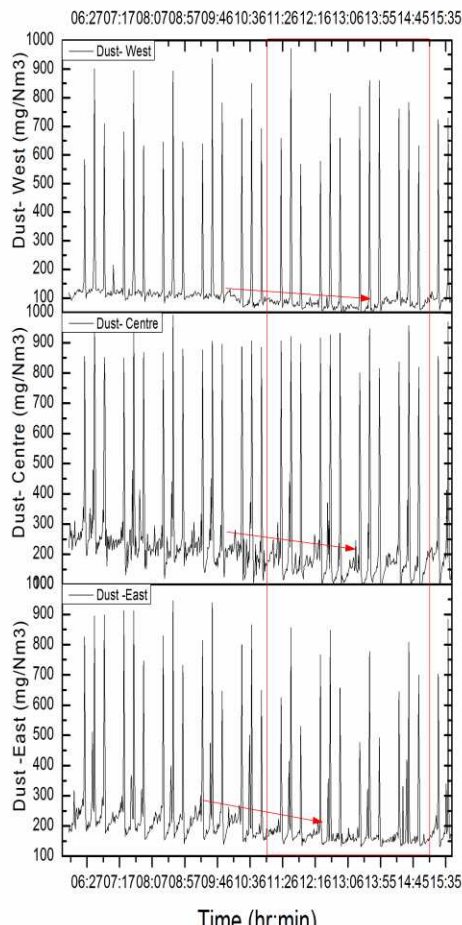
Figure 4. Effect of the injection of Silanite™ on the loss on ignition calculated for collected fly ash samples temperature.

13%; 5%; 20% less dust concentration compared to coal baseline on E,C&W legs



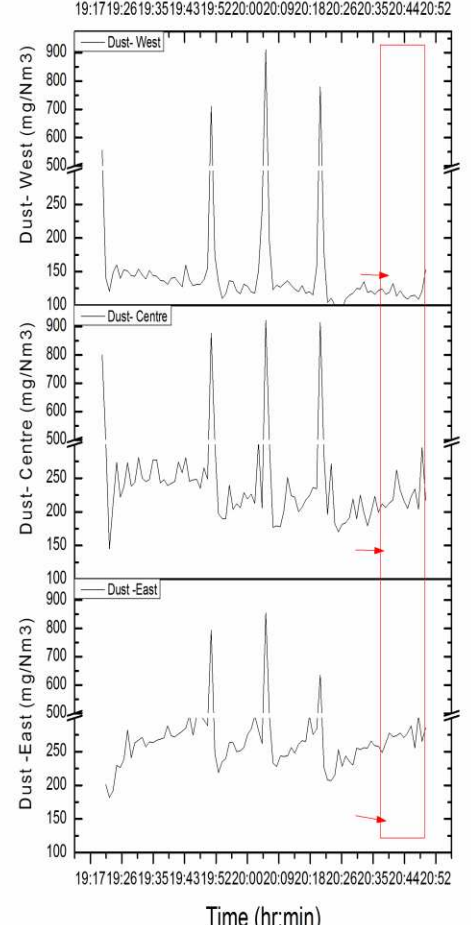
45min Full Scale Trial

17%; 18%; 17% less dust concentration compared to coal baseline on E, C&W legs



7-8 hour Full Scale Trial

5%; 19%; 28% less dust concentration compared to coal baseline on E, C&W legs



1 hour Full Scale Trial

Figure 5. Effect of the injection of Silanite™ on Dust concentration post ESPs.

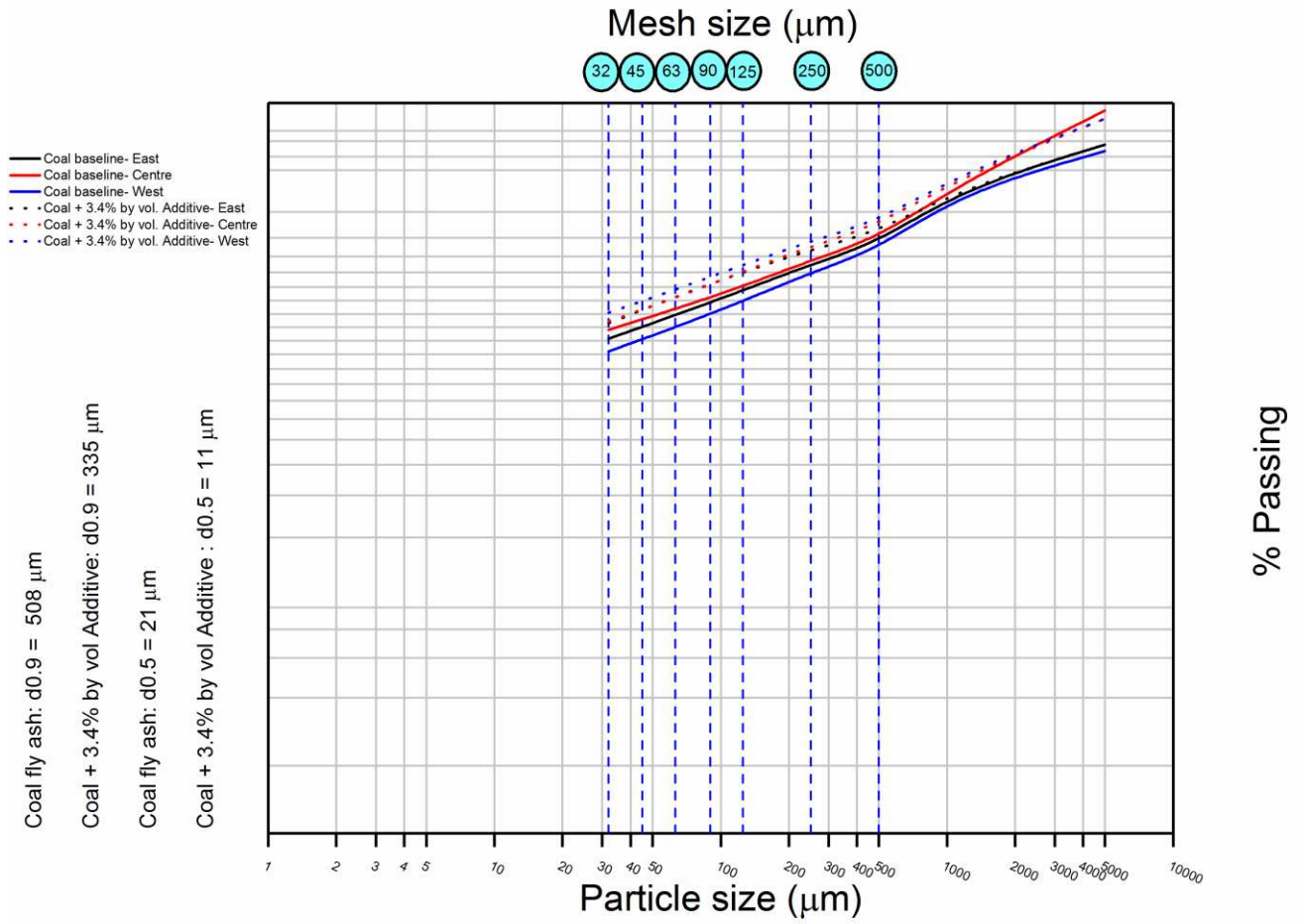


Figure 6. Air jet sieve- Rosin Rammler Distribution with and with Silanite™ injection.

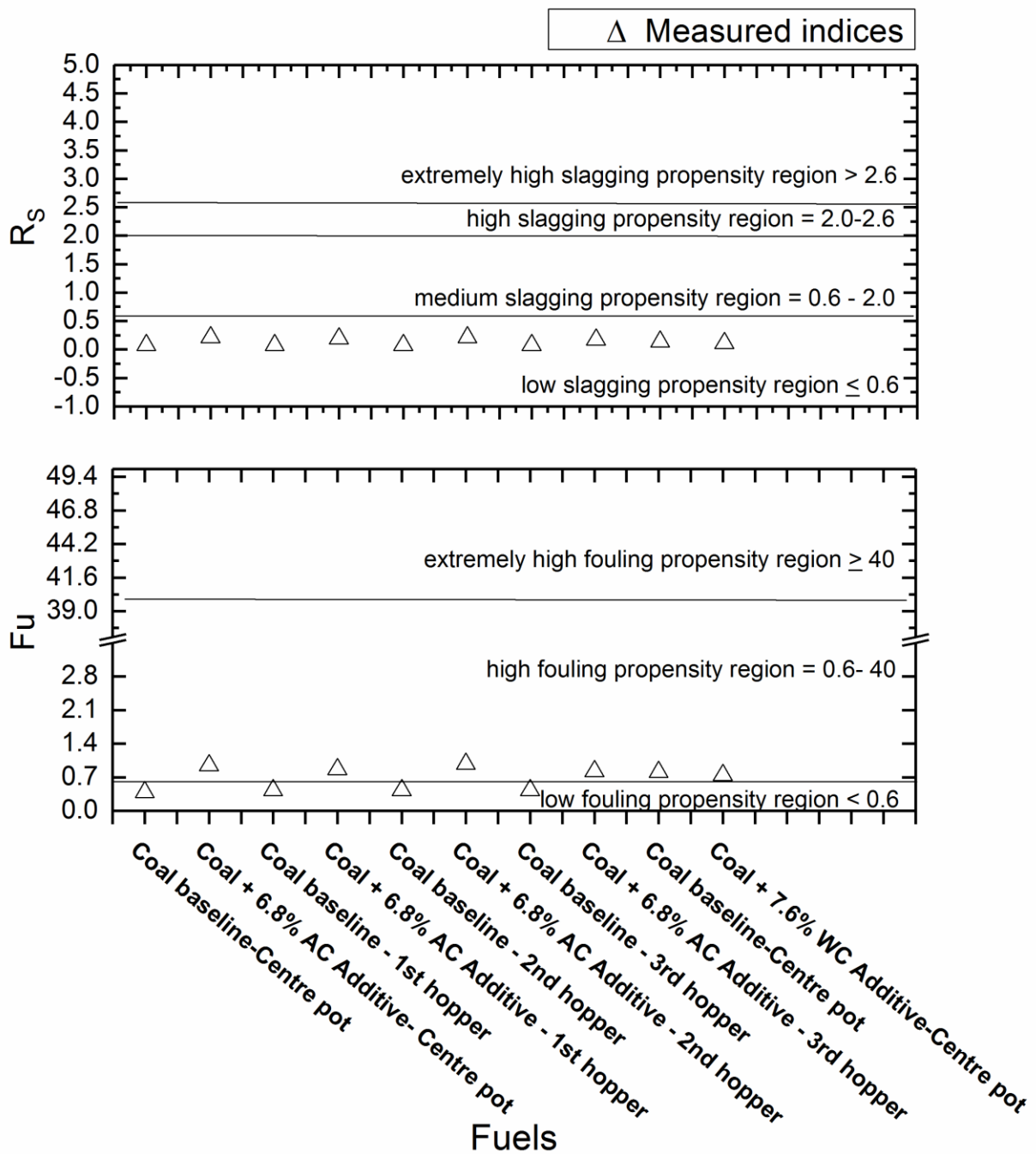


Figure 7. Slagging and fouling indices with and with Silanite™ injection.

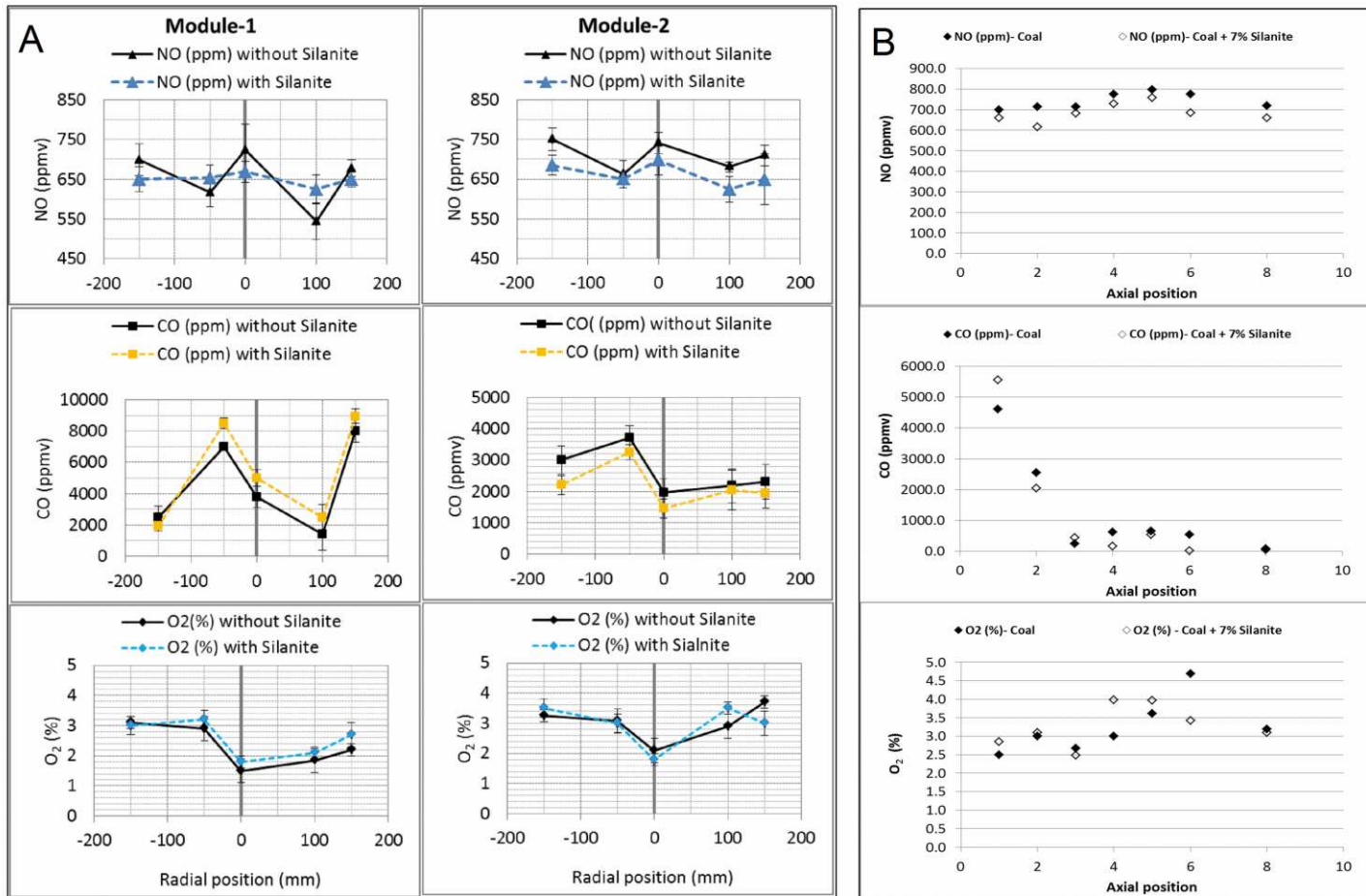


Figure 8. a) Radial profiles with a test sub-bituminous coal imported from outside UK; b) Axial profiles (NO, CO and O₂).

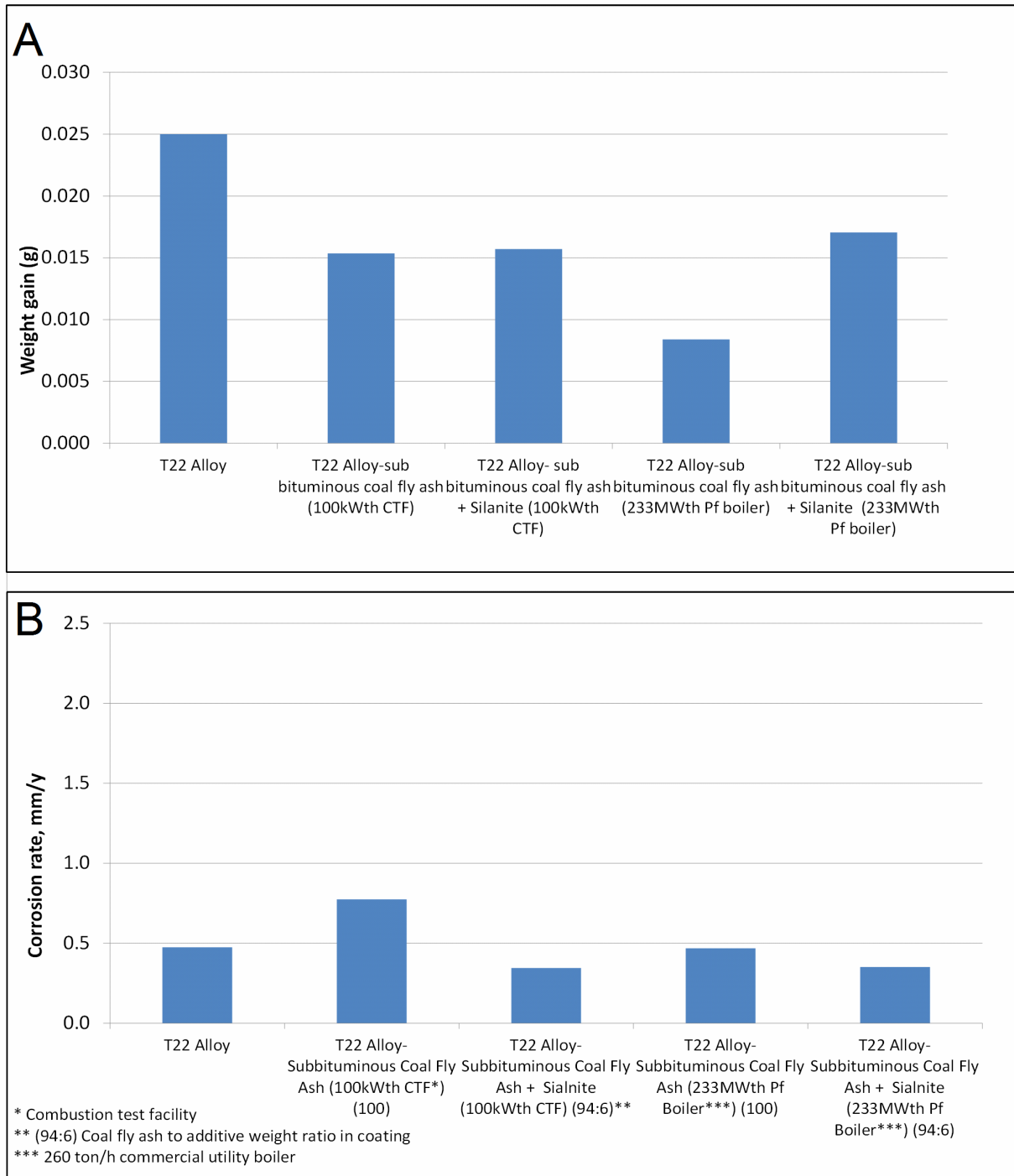


Figure 9. a) Mass gain b) Corrosion rate: after 1000h exposure of the T22 alloy specimens.

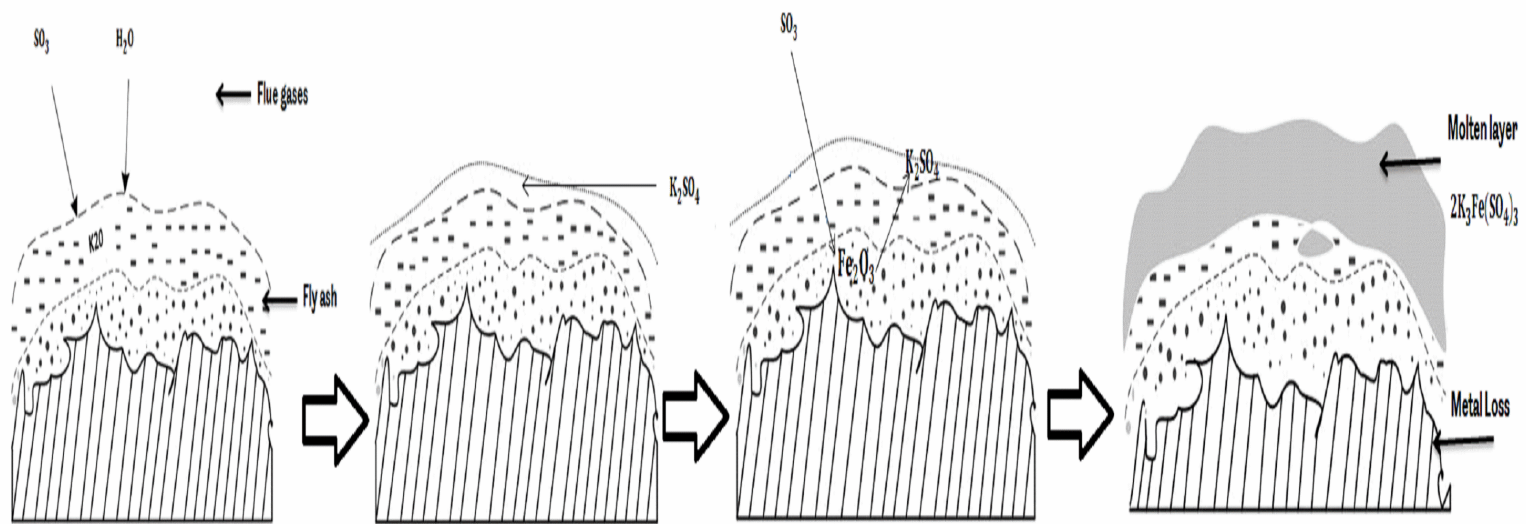
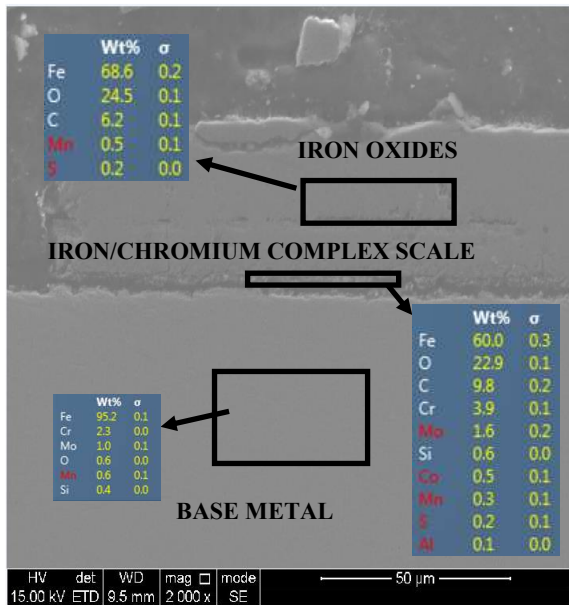
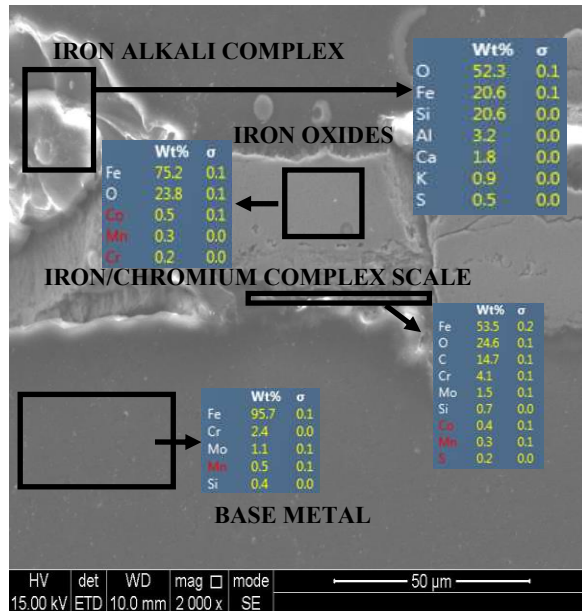


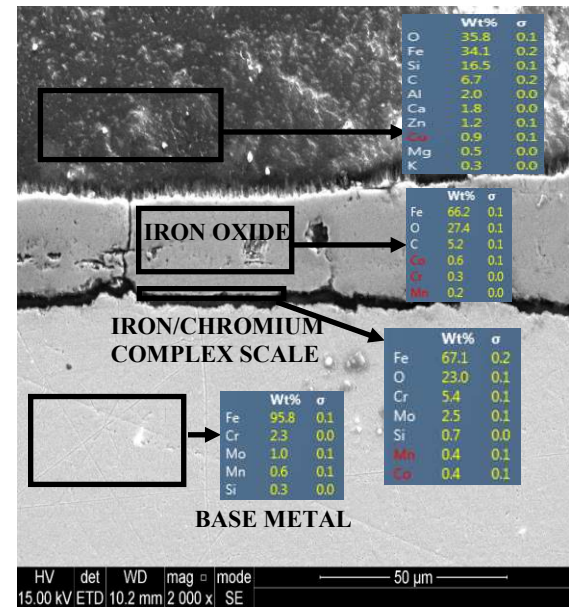
Figure 10. The morphological pictorial representation of the sulphidation reactions.



a) SEM/EDS-Cross-section non-coated T22



b) SEM/EDS-Cross-section Coal fly ash coated T22



c) SEM/EDS-Cross-section Silanite™ +Coal fly ash coated T22

Figure 11. SEM /EDS of the cross-sectional view of the 1000h exposure non –coated and coated T22 alloy samples.

Table 1 Analysis of Silanite™ and UK-based utility Coal & collected fly ash.

Ultimate Analysis as received, %	UK-Utility Coal	Silanite™
C	66.00	
H	4.60	
N	2.53	
O (diff)	8.90	-
S	0.02	
H ₂ O	6.00	
Ash	11.95	
Proximate Analysis as received, %	UK-Utility Coal	Silanite™
Volatile Matter	17.08	-
Fixed Carbon	64.97	-
Ash	11.95	97.5
Moisture	6.00	2.50
Net Calorific Value, MJ/kg	27.04	0
Air Jet Sieving	UK-Utility Coal	Silanite™
d(0.1) (µm)	11.5	2.5
d(0.50) (µm)	62.5	12
d(0.9) (µm)	181	26
X-Ray fluorescence analysis (% normalized) of the collected fly ash as part of commercial scale test	UK-Utility Coal fly ash	UK- Utility Coal - Silanite™ fly ash
SiO ₂	43.79	37.13
TiO ₂	0.81	0.6
Al ₂ O ₃	18.19	14.45
Fe ₂ O ₃	5.15	21.09
MnO	0.04	0.05
MgO	1.63	1.9
CaO	4.91	3.9
Na ₂ O	0.29	0.46
K ₂ O	1.7	1.32
P ₂ O ₅	0.45	0.43
SO ₃	0.883	0.93
ZnO	0.018	0.34
CuO	0.0087	0.26
PbO	0.0058	0.08
Cr ₂ O ₃	116 µg/g	209 µg/g
LOI + Others	22.12	17.06

Table 2 Timeline based protocol during the test.

1.	Soot blowing completion before the test
2.	Coal mill (Babcock type 6.3E9 vertical) 6-A being inoperative due to the maintenance purposes, hence, 6-B and 6-C utilised for maintained coal flows. Coal mill-B load reduced from 12.4t t.h-1 to 11.38 t.h-1 from 06:00 to 06:45. Coal mill-C load was reduced from 12.4 t.h-1 to 12t.h-1 from 06:00 to 19:19.
3.	Electrostatic precipitators (ESPs) cleaned by ash recovery vacuum system.
4.	Boiler steady load started 07:00 to 10:20.
5.	Blow down left open at ¼ turn on valve, conductivity 16µs (agreed with Parson Brinckerhoff to maintain blow down at ¼ turn throughout the test with or without additive). The blow down flow rate was not measured; its impact on the net change in net boiler efficiency improvement is cancelled for both with and without additive due to consistent ¼ turn opening.
6.	Pf samples taken during the coal steady baseline.
7.	Fly ash recovery system switched off from control room at 07:57
8.	The fly ash hoppers underneath ESPs emptied by ash recovery vacuum system 08:30.
9.	Fly ash and bottom ash samples collection completed by 09:30.
10.	The initial steady base line between 07:00 to 10:10.
11.	Fly ash hopper underneath ESPs by ash recovery vacuum system 10:15.
12.	Additive (3.4% by vol. i.e. 1.59 t.h-1) injection started at 10:20. The injection rate was selected in agreement with Sembcorp plant operators and PB's Inspection team.
13.	Pf samples for coal and additive mixture completed 13:20.
14.	Fly ash and bottom ash samples completed by 14:50.
15.	Additive injection stopped at 15:00.
16.	Test concluded at 15:00
17.	The ending baseline was recorded but due to steam demand from customers, coal mills loads were changed resulting in changed ending coal baseline.

Table 3 Net boiler efficiency calculation with and without Silanite™.

Calculation of Efficiency of Water tube Boilers with out ADDITIVE		HEAT OUTPUT					
$\eta(N)B = Q_u/Q_{in}Z_{tot}$	Q_u	Useful heat flow (kw)					
$\eta(N)B =$ Net usefull Boiler Efficiency	mST= is the live steam flow	205 tons/hr	56.96	kg/s			
$Q(N) =$ Net heat flow (kW)	mSS= is the spray water mass flow for main steam attemperator	16.2 tons/hr	4.50	kg/s			
$Q_N =$ Useful heat flow (kW)	hFW = is the enthalpy of feed water	Temp. 199.6 deg C Press. 1841.16 psig	857.24	kJ/kg			
$Z_{tot} =$ Total Heat input	hST= is the enthalpy of live steam	Temp. 520.6 deg C Press. 1583.58 psig	3413.81	kJ/kg			
	hSS= is the enthalpy of spray water upstream of main steam attemperator	Temp. 200.34 deg C	858.14	kJ/kg			
$\eta =$	80.82	QN is calculated as follows		Press. 2136.25 psig			
	$Q_N = mST(hST-hFW) + mSS(hFW-hSS)$		145607.59 kW	524.2 GJ/hr			
HEAT INPUT FROM FUEL							
$Q_{in}ZF = mF * [(H(N)+hF)/(1-U) + \mu AS * h(N)AS + J(N)A]$							
	$H(N)_{tot} = [H(N)+hF]/[1-U] + J(N)A$		27656.76174	kJ/kg			
	H(N)= is the NCV of fuel at reference temperature tr=		27043	kJ/kg			
	hF= is the enthalpy of fuel = hf=cf*(tf-tr)=		-6.18	kJ/kg			
	cF= is the specific heat of the fuel=		1.03	kJ/kgK			
	tf= is the temperature of fuel=		19.00	oC			
	tr= is the temperature of reference=		25.00	oC			
	$U = \gamma Ash (1-v)/(1-\gamma Ash - \gamma H2O) [uSL/(1-uSL) nSL + uFA/(1-uFA) \eta FA]$		0.024				
	γAsh Ash content of fuel		0.120				
	$\gamma H2O$ Water content of fuel		0.060				
	v Ash Volatile matter, p.37 -EN12952 suggest 0.05		0.050				
	based on 10% unburned combustible in slag	uSL Unburned combustible content of slag	0.001				
	measured from sample	uFA Unburned combustible content of fly ash	0.150				
		ηFA fly ash retention efficiency	0.989				
		mFu= unburned fuel mass flows	0.19	kg/s			
		mFo= supplied fuel mass flow	23.39	6.50	kg/s		
	based on 1% of ash via coal input	mSL= Mass of slag	0.008	kg/s			
		ηSL slag collection efficiency Eq 8.3-41	0.011				
	J(N)A= is the enthalpy of combustion air due to NCV calculation=		-52.04	kJ/kg			
	$J(N)A = \mu A * cpA (tA - tr)$		8.09				
	μA is the combustion air mass to fuel mass ratio		189.16	52.55	kg/s		
	Combustion air mass flow=		23.39	6.50	kg/s		
	Fuel mass flow=		1.01	kJ/kgK			
	cpA= specific heat of air between 25-150oC		18.64	oC			
	tA= is the air temperature at envelope boundary		25	oC			
	tr= is the reference temperature		23.39	6.50	kg/s		
	mF= is the fuel mass flow						
	$Q(N)ZF = mF * H(N)_{tot}$		179681.552	kJ/s			
HEAT CREDIT							
$Q_{NZ} = PM + P + Q_{SAE} + mAS * h(N)AS$ QNZ= is the total heat credit							
	PM= is the Pulverizer power	kW	296.2	measured			
	P= is the power of any other motors	kW	183.2	measured			
	$Q_{NZ} =$		479.402				
TOTAL HEAT INPUT							
	$Q_{NZtot} = Q_{NZZF} + Q_{NZ}$		180160.95 kW	648.6 GJ/hr			

Calculation of Efficiency of Water tube Boilers with ADDITIVE		HEAT OUTPUT					
$\eta(N)B = Q_u/Q_{in}Z_{tot}$	Q_u	Useful heat flow (kw)					
$\eta(N)B =$ Net usefull Boiler Efficiency	mST= is the live steam flow	205.385 tons/hr	57.05	kg/s			
$Q(N) =$ Net heat flow (kW)	mSS= is the spray water mass flow for main steam attemperator	15.7355 tons/hr	4.37	kg/s			
$Q_N =$ Useful heat flow (kW)	hFW = is the enthalpy of feed water	Temp. 199.2 deg C press= 1841.17 psig	857.24	kJ/kg			
$Z_{tot} =$ Total Heat input	hST= is the enthalpy of live steam	Temp. 520.9 deg C press= 1581.82 psig	3413.81	kJ/kg			
	hSS= is the enthalpy of spray water upstream of steam attemperator	Temp. 200.62 deg C	858.14	kJ/kg			
$\eta =$	81.87	QN is calculated as follows		Press. 2136.25 psig			
	$Q_N = mST(hST-hFW) + mSS(hFW-hSS)$		145851.724 kW	525.1 GJ/hr			
HEAT INPUT FROM FUEL							
$Q_{in}ZF = mF * [(H(N)+hF)/(1-U) + \mu AS * h(N)AS + J(N)A]$							
	$H(N)_{tot} = [H(N)+hF]/[1-U] + J(N)A$		27346.90356	kJ/kg			
	H(N)= is the NCV of fuel at reference temperature tr=		27043	kJ/kg			
	hF= is the enthalpy of fuel = hf=cf*(tf-tr)=		-6.18	kJ/kg			
	cF= is the specific heat of the fuel=		1.03	kJ/kgK			
	tf= is the temperature of fuel=		19.00	oC			
	tr= is the temperature of reference=		25	oC			
	$U = \gamma Ash (1-v)/(1-\gamma Ash - \gamma H2O) [uSL/(1-uSL) nSL + uFA/(1-uFA) \eta FA]$		0.013				
	γAsh Ash content of fuel		0.120				
	$\gamma H2O$ Water content of fuel		0.060				
	v Ash Volatile matter, p.37 of EN12952 suggest 0.05		0.050				
	based on 10% unburned combustible in slag	uSL Unburned combustible content of slag	0.001				
	measured from sample	uFA Unburned combustible content of fly ash	0.087				
		ηFA fly ash retention efficiency	0.989				
		mFu= unburned fuel mass flows	0.15	kg/s			
		mFo= supplied fuel mass flow	23.39	6.50	kg/s		
	based on 1% of ash via coal input	mSL= Mass of slag	0.008	kg/s			
		ηSL slag collection efficiency Eq 8.3-41	0.011				
	J(N)A= is the enthalpy of combustion air due to NCV calculation=		-48.98	kJ/kg			
	$J(N)A = \mu A * cpA (tA - tr)$		8.10				
	μA is the combustion air mass to fuel mass ratio		189.33	52.59	kg/s		
	Combustion air mass flow=		23.39	6.50	kg/s		
	Fuel mass flow=		1.01	kJ/kgK			
	cpA= specific heat of air between 25-150oC		19.02	oC			
	tA= is the air temperature at envelope boundary		25	oC			
	tr= is the reference temperature		23.39	6.50	kg/s		
	mF= is the fuel mass flow						
	$Q(N)ZF = mF * H(N)_{tot}$		177665.231	kJ/s			
HEAT CREDIT							
$Q_{NZ} = PM + P + Q_{SAE} + mAS * h(N)AS$ QNZ= is the total heat credit							
	PM= is the Pulverizer power	kW	295.1	measured			
	P= is the power of any other motors	kW	182.8	measured			
	$Q_{NZ} =$		477.965				
TOTAL HEAT INPUT							
	$Q_{NZtot} = Q_{NZZF} + Q_{NZ}$		178143.1962 kW	641.3 GJ/hr			

Table 4 Dust concentration (mg.Nm⁻³) east-center and west bound legs of the boiler.

	Dust (mg.Nm ⁻³)	particulate-East	Dust Centre (mg.Nm ⁻³)	particulates- West (mg.Nm ⁻³)
Coal fly ash	246.3		266.9	148.7
Standard Deviation for coal fly ash calculation	139		158	138
Coal + 6.8% AC Silanite fly ash	206.2		224.5	122.3
Standard Deviation for coal + 6.8% AC Silanite fly ash calculation (-)	133		188	157
Dust reduction w.r.t coal baseline (%)	16.25		15.89	17.76

Table 5 Slagging and fouling indices based on the X-Ray fluorescence (XRF) analysis.

Metal in ash reported as %	Sample 7- ESPs coal fly ash 1 st Field / 1 st hopper	Sample 10- ESPs coal fly ash + AC Silanite 1 st Field / 1 st hopper	Sample 8- ESPs coal fly ash 1 st Field / 2 nd hopper	Sample 11- ESPs coal fly ash + AC Silanite 1 st Field / 2 nd hopper	Sample 9- ESPs coal fly ash 1 st Field / 3 rd hopper	Sample 12- ESPs coal fly ash + AC Silanite 1 st Field / 3 rd hopper	Sample 16- Bottom coal fly ash	Sample 17- Bottom coal + 6.8% AC Silanite fly ash
SiO ₂	43.25	38.78	43.79	37.13	44.33	39.27	15.42	15.88
TiO ₂	0.79	0.63	0.81	0.60	0.81	0.64	0.37	0.39
Al ₂ O ₃	18.24	15.03	18.19	14.45	18.22	15.31	5.80	5.86
Fe ₂ O ₃	5.00	18.92	5.15	21.09	5.09	17.70	3.81	7.24
MnO	0.04	0.05	0.04	0.05	0.04	0.05	0.03	0.02
MgO	1.68	1.38	1.63	1.90	1.67	1.71	0.06	0.07
CaO	4.70	4.13	4.91	3.90	4.86	4.11	3.21	2.85
Na ₂ O	0.29	0.41	0.29	0.46	0.29	0.41	0.20	0.24
K ₂ O	1.72	1.39	1.70	1.32	1.70	1.40	0.68	0.65
P ₂ O ₅	0.46	0.42	0.45	0.43	0.47	0.44	0.14	0.18
SO ₃	0.9070	0.9790	0.8830	0.93	0.9190	0.92	0.906	1.175
ZnO	0.0192	0.2810	0.0180	0.34	0.0170	0.25	0.009	0.035
CuO	0.0088	0.2239	0.0087	0.26	0.0083	0.20	0.008	0.063
PbO	0.0059	0.0707	0.0058	0.08	0.0051	0.06	0.002	0.008
B/A	0.22	0.48	0.22	0.55	0.21	0.46	0.37	0.50
R(B/A)	0.19	0.45	0.19	0.52	0.19	0.43	0.33	0.47
Rs	0.08	0.19	0.08	0.21	0.08	0.17	0.13	0.23
Fu	0.43	0.87	0.43	0.98	0.43	0.83	0.32	0.44

Table 6 Ash fusibility temperatures.

Sample ID	Description	Slagging index calculated on the basis of Deform. Temp and hemi. temp				
		Ash fusibility temperatures				
		Fs ^a = (4DT + HT)/5	Deformation temperature	Sphere temperature	Hemisphere temperature	Flow temperature
		°C [K]	°C [K]	°C [K]	°C [K]	°C [K]
Sample 7	ESP's coal fly ash 1 st field / 1 st hopper	1254 [1527.15]	1240 [1513.15]	1260 [1533.15]	1310 [1583.15]	1330 [1603.15]
Sample 10	ESP's coal fly ash + 6.8% AC Silanite 1 st field / 1 st hopper	1258 [1531.15]	1240 [1513.15]	1260 [1533.15]	1330 [1603.15]	1360 [1633.15]
Sample 8	ESP's coal fly ash 1 st field / 2 nd hopper	1259 [1532.15]	1240-1250 [1513.15-1523.15]	1260 [1533.15]	1310-1320 [1583.15-1603.15]	1350 [1623.15]
Sample 11	ESP's coal fly ash + 6.8% AC Silanite 1 st field / 2 nd hopper	1258 [1531.15]	1240 [1513.15]	1260 [1533.15]	1330 [1603.15]	1360 [1633.15]
Sample 9	ESP's coal fly ash 1 st field / 3 rd hopper	1258 [1531.15]	1240 [1513.15]	1270 [1543.15]	1330 [1603.15]	1340 [1613.15]
Sample 12	ESP's coal fly ash + 6.8% AC Silanite 1 st field / 3 rd hopper	1251 [1524.15]	1230 [1503.15]	1260 [1533.15]	1330-1340 [1603.15-1613.15]	1360 [1633.15]
Sample 13	AC Silanite	1306 [1579.15]	1280 [1553.15]	1350 [1623.15]	1410 [1683.15]	1420 [1693.15]
Sample 14	WC Silanite	1342 [1615.15]	1320 [1593.15]	1390 [1663.15]	1430 [1703.15]	1440 [1713.15]
Sample 19C	Cegrit Pot Coal fly ash	1270 [1543.15]	1260 [1533.15]	1260 [1533.15]	1310 [1583.15]	1330-1340 [1603.15-1613.15]
Sample 20C	Cegrit Pot Coal fly ash + 6.8% AC Silanite	1252 [1525.15]	1240 [1513.15]	1250-1260 [1523.15-1533.15]	1300 [1573.15]	1340-1350 [1613.15-1623.15]
Sample 21C	Cegrit Pot Coal fly ash	1252 [1525.15]	1240 [1513.15]	1260 [1533.15]	1300 [1573.15]	1340 [1613.15]
Sample 22C	Cegrit Pot Coal fly ash + 8% AC Silanite	1248 [1521.15]	1230 [1503.15]	1250 [1523.15]	1320 [1593.15]	1350 [1623.15]
Sample 23C	Cegrit Pot Coal fly ash	1244 [1517.15]	1230 [1503.15]	1250 [1523.15]	1300 [1573.15]	1320 [1593.15]
Sample 24C	Cegrit Pot Coal fly ash + 8% WC Silanite	1256 [1529.15]	1240 [1513.15]	1260 [1533.15]	1320 [1593.15]	1330 [1603.15]

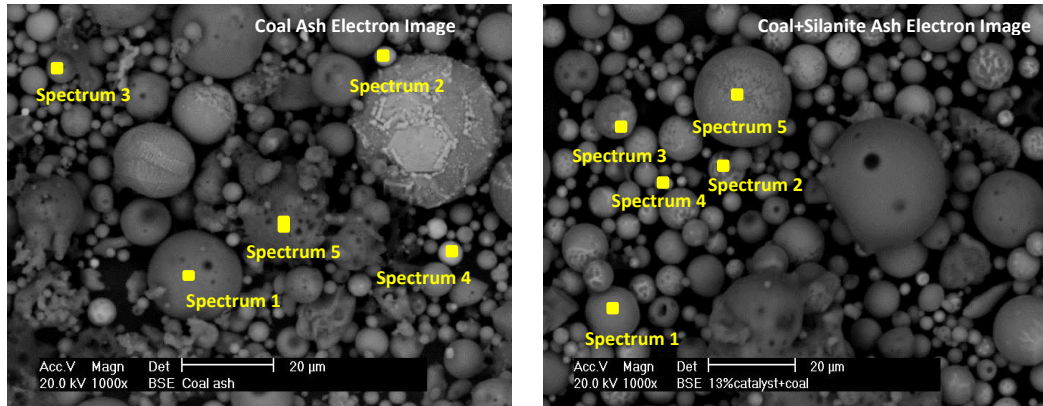
^a Fs= Slagging index proposed by Gary and Moore (R.J. Gray, G.F. Moore, Burning the sub-bituminous coals of Montana and Wyoming in large utility boilers, ASME paper (1974) p. 74-WA/FU-1)

Medium slagging propensity ; $1232\text{ }^{\circ}\text{C}$ [1505.15 K] < Fs < $1342\text{ }^{\circ}\text{C}$ [1615.15 K]

High slagging propensity; $1052\text{ }^{\circ}\text{C}$ [1325.15 K] < Fs < $1232\text{ }^{\circ}\text{C}$ [1505.15 K]

Severe high slagging propensity; $1052\text{ }^{\circ}\text{C}$ [1325.15 K]

Table 7 SEM/ EDS of the coal and coal+ Silanite ash.



Element Weight %	Coal ash Analysis (normalised spectrum with 5 no of iterations)				
	Spectrum 1	Spectrum 2	Spectrum 3	Spectrum 4	Spectrum 5
C	0.14	3.86	6.36	4.98	53.90
O	57.00	46.23	58.99	40.80	33.72
Na	0.58	-	0.62	-	0.18
Mg	1.13	4.65	0.59	1.00	0.32
Al	9.91	4.32	11.82	1.61	2.87
Si	25.62	7.44	18.51	2.61	6.30
K	2.03	-	1.74	-	0.49
Ca	1.91	1.67	0.25	6.89	0.78
Ti	0.34	-	0.36	-	0.20
Fe	1.61	30.7	0.78	39.51	1.11
P	-	0.40	-	0.78	-
Mn	-	0.74	-	1.83	-
S	-	-	-	-	0.15
Element Weight %	Coal + 13% Silanite ash Analysis (normalised spectrum with 5 no of iterations)				
	Spectrum 1	Spectrum 2	Spectrum 3	Spectrum 4	Spectrum 5
C	3.66	5.14	10.73	4.50	5.02
O	46.64	39.43	47.56	53.46	44.51
Na	0.57	-	0.59	0.77	0.55
Mg	0.31	0.41	0.40	0.61	0.48
Al	1.90	1.88	1.90	4.17	1.80
Si	18.83	13.82	14.01	17.16	16.54
K	0.41	0.38	0.34	0.83	0.28
Ca	1.09	1.96	1.22	2.70	1.44
Ti	-	-	-	0.31	-
Fe	26.29	36.33	23.25	14.82	29.08
P	-	-	-	0.36	-
Mn	-	-	-	-	0.30
S	-	-	-	0.31	-
Cu	0.29	0.66	-	-	-